Interfacing Solid-State Nanopores with Gel Media to Slow DNA Translocations

Matthew Waugh

THESIS SUBMITTED IN PARTIAL FULFILLMENT OF THE REQUIREMENTS

FOR THE DEGREE OF

MASTER OF SCIENCE

In the Faculty of Graduate and Postdoctoral Studies (Physics)

Table of Contents

Abstract

One of the most crucial steps towards nanopore-based nucleic acid analysis is extending the dwell time of DNA molecules within the sensing region of the nanopore. I address this issue by interfacing solid-state nanopores with gel media, which sterically hinders translocating DNA molecules, increasing dwell times. Specifically, my experimental results focus on two reptation regimes: when the DNA molecule is flexible on the length scale of the gel pore, and when the DNA molecule is inflexible on the length scale of the gel pore. The first regime is achieved through the use of agarose gel and 5 kbp dsDNA fragments, and produces a wide distribution of translocation times, spanning roughly three orders of magnitude. The second regime is achieved through the use of polyacrylamide gel and 100 bp dsDNA fragments, and displays a shift in translocation times by an order of magnitude while maintaining a tight distribution.

Résumé

Une étape cruciale pour l'analyse d'acide nucléique à l'aide de nanopores est d'allonger la durée de séjour des molécules d'ADN à proximité de la région de détection du nanopore. J'aborde ce problème en superposant un nanopore à l'état solide avec un médium gélatineux, ce qui induit un blockage stérique et augmente le temps de translocation. Spécifiquement, mes résultats expérimentaux focalisent sur deux régimes de reptation: lorsque la molécule est flexible ou à l'échelle du pore du gel ou lorsqu'elle est inflexible à l'échelle du pore du gel. Le premier régime est atteint avec l'usage de gel d'agarose et de fragments d'ADN à doubles brins de 5 kpb et produit une large distribution de temps de translocation s'étendant sur approximativement 3 ordres de grandeur. Le deuxième régime est atteint avec

l’usage de gel de polyarylamide et d’ADN à doubles brins de 100 pb et démontre un décalage de temps de translocation d’une ordre de grandeur tout en maintenant une distribution étroite.

Statement of Originality

The content presented in this document is, to the best of the author's knowledge, the product of original work performed by the author at the University of Ottawa under the supervisor of Prof. Vincent Tabard-Cossa.

Chapter 2 is a reproduction of the following publication:

> **Waugh, M.**, Carlsen, A., Sean, D., Slater, G., Briggs, K., Kwok, H., and Tabard-Cossa, V. 2015. *Interfacing Solid-State Nanopores with Gel Media to Slow DNA Translocations*. Electrophoresis. *Accepted.*

In addition, parts of Section 1.7, 1.11, and 3.1 are borrowed from the publication above.

I was also given the opportunity to present my work at the 58th annual Biophysical Society Meeting in San Francisco, California in February 2014;

> **Waugh, M.** and Tabard-Cossa, V. 2014. *Translocation Kinetics of DNA through Nanopores Interfaced with Agarose Gel*. Biophysical Society Meeting.

In partial fulfilment of the requirements for the degree of Master of Science (Physics) at the University of Ottawa, I presented my work at the Ottawa Carleton Institute for Physics graduate student symposium:

> **Waugh, M**. and Tabard-Cossa, V. 2014. *Interfacing solid-state nanopores with gel media to slow DNA translocations.* Ottawa Carleton Institute of Physics.

Other contributions made by the author and not included in this thesis have helped secure publications. These are listed below;

Briggs, K., Charron, M., Kwok, H., Le, T., Chahal, S., Bustamante, J., **Waugh, M**., and Tabard-Cossa, V. 2015. *Kinetics of Nanopore Fabrication During Controlled Breakdown of Dielectric Membranes in Solution*. Nanotechnology. 26 (8), 084004.

Kwok, H., **Waugh, M.**, Bustamante, J., Briggs, K., and Tabard-Cossa, V. 2014. *Long Passage Times of Short ssDNA Molecules through Metallized Nanopores Fabricated by Controlled Breakdown.* Advanced Functional Materials. 24 (48), 7745-7753.

Statement of Contributions

The design of the PEEK cells was the work of the author, as was the assembly of the set-up. The nanopore fabrication circuit was designed by Prof. Vincent Tabard-Cossa and Dr. Harold Kwok, and built by Lukasz Andrzejewski. The LabView routines for data acquisition and analysis were versions of code provided by Prof. Vincent Tabard-Cossa or Dr. Harold Kwok. Figures 1.2-1.4, 1.6, 1.8 and 1.10-1.13 were reproduced with permission from the cited source. Figure 2.1 was the work of David Sean. All other figures were the work of the author. Writing of the draft of the manuscript was done by the author and Dr. Autumn Carlsen. All experiments, sample preparation and analysis were performed by the author. David Sean helped with discussions relating to the transport of DNA through a gel. The manuscript was written and/or edited by the author, Dr. Autumn Carlsen, Prof. Vincent Tabard-Cossa, David Sean and Prof. Gary W. Slater.

List of Figures

Legend

R_C	Convection length
l_D	Debye length
d_{gel}	Diameter of gel pore
dsDNA	Double stranded DNA
EDL	Electric double layer
L_{DNA}	Length of DNA
L_P	Persistence length
R_g	Radius of gyration
ssDNA	Single stranded DNA
TEM	Transmission electron microscope

Acknowledgements

Throughout my time as a Master's student there have been innumerable people that helped me stay focused, overcome obstacles, and help me truly enjoy my time in the Tabard-Cossa lab. This is an inexhaustive list that highlights but a few.

Firstly, above all I would like to acknowledge Prof. Vincent Tabard-Cossa. His ability to support, guide and remain patient was admirable, and made perseverance and success possible. I sincerely appreciate how he was always available to answer questions, which made it easy to gain a deep understanding of nanopores in the early stages of my degree. Without his optimistic yet understanding attitude, this work would have been much more difficult.

I would also like to thank the members of my lab, in no particular order, for their contributions to my research, as well as making the work interesting, if not fun. To begin, Kyle Briggs has always been there for useful discussions as well as entertainment (if you insist on taking your shirt off, at least it could be used as a wind-net). Eric Beamish, too, has helped with many useful discussions and even more useless ones. I'd also like to recognize Radin Tahvildari for always being so quick to lend a hand, and Dr. Harold Kwok, Jose Bustamente and Dr. Autumn Carlsen for all their help and support. Additionally, both Prof. Gary Slater and David Sean contributed immensely with their discussions, suggestions, and simulations.

Finally, I would like to thank Mom, Ron, Ally, Amy and Dad for their support during the entirety of my degree. Lastly, Ellen, while you didn't help with my degree in any tangible way, you didn't actively seek out ways to sabotage it either, making you neutral to this work.

1 Introduction

Across the globe and throughout history, one of the most common goals amongst nearly all people has been to cure, sooth and prevent illness. While it is difficult to define exactly what constitutes modern medicine and when it began, credit often goes to the ancient Egyptians. Remarkably, around year 2750 BCE, they performed what is considered to be the first confirmed surgery [1]. By today's standards their practices were likely rudimentary, but our goals have remained largely the same; to elongate life and prevent disease while causing as little collateral damage to the body as possible.

Unfortunately, while it is often easy to observe symptoms of malaise, it can be extremely difficult to treat them. This is because a person is a network of unfathomably complex chemical and electrical signals which occur all over the body for every second of their existence. It is these signals that allow for the necessary physiological activities we often take for granted, like allowing our muscles to contract, our eyes to see and body to know when it is hungry. However, while these complexities make life easier when they function, they make it very difficult to identify problems when things go awry. One of the most common issues is that many different ailments manifest themselves similarly, thus clouding our ability to diagnose and treat an illness. To further complicate matters, each person's body can react differently to treatment, meaning what works for one person may not work for another. Taken together, these two issues can make it very difficult for a medical professional to alleviate a given illness.

As a result, a relatively new idea in medicine has come into favour, where each person is treated individually based on their DNA, RNA and protein makeup. This approach has been termed *personalized medicine,* and is very promising. Theoretically, by looking at the building blocks that make up each person, a researcher would obtain an up-to-date status report on what a patient's body is doing, and why troubles are occurring. This method of diagnosis is beneficial because it eliminates the reliance on macroscopic manifestations of a disease, while simultaneously allowing for the investigation into any potential problems in treatment options. With more reliable diagnosis techniques, medical professionals could make a more informed treatment recommendation, potentially saving both time and resources on the part of the patient, the doctor and the medical institution.

In order to maximize the amount of information obtained from personalized medicine, we turn to the central dogma of molecular biology, which is presented in Figure 1. Essentially, it states that biological information contained within either DNA or RNA can be replicated to form exact copies, or can be converted from DNA to RNA or from RNA into proteins (it is possible, although rare, to convert DNA into protein, or RNA into DNA) [2]. Importantly, since DNA contains all of the information a cell needs to grow, survive and reproduce, determining the sequence of a genome will yield information similar to that of looking at RNA or proteins directly. Additionally, DNA contains extra information not transferred to RNA or proteins, and is contained neatly in a long strand, thus adding convenience and making it a good candidate for use in personalized medicine.

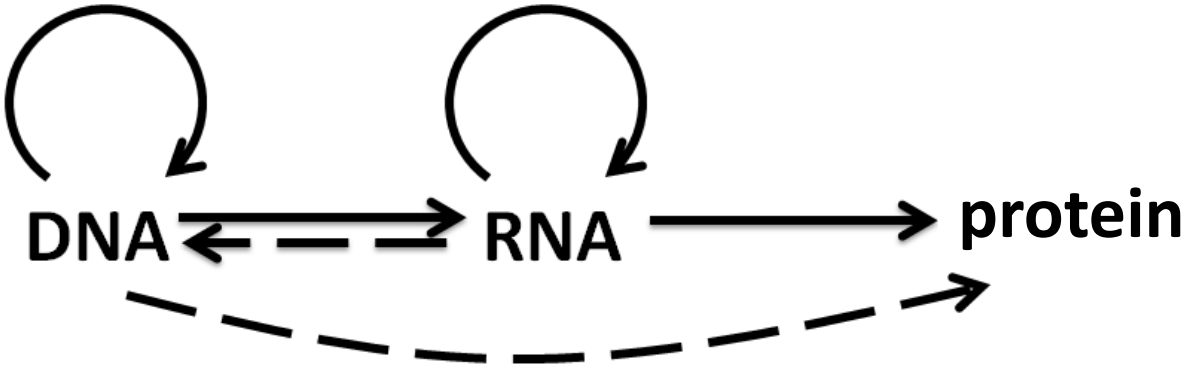

Figure 1.1. Representation of the central dogma of molecular biology. DNA can either be replicated or transfer information into RNA, as represented by the circular and linear arrow, respectively. RNA can either be replicated or transfer its information into protein form, as represented by the circular and linear arrow, respectively. While possible, the transfer of information from RNA to DNA or from DNA to protein, it is very rare and not typically found within healthy individuals.

As is evident from Figure 1.1, in theory a researcher should be able to obtain all the information contained within a person's cells by looking at their DNA makeup. While this is very difficult in practice, DNA still provides valuable information, and is the basis of personalized medicine. In fact, for certain well known diseases, this is already done. For instance, one example that highlights the usefulness of interrogating a person's DNA is the *KRAS* gene. The *KRAS* gene codes for a protein that is tasked with cellular signal transduction, and is essential for healthy human life. If a person is unlucky enough to have a single nucleotide inserted/deleted/mutated in a critical area of this gene, severe health problems can arise. A mutation of the *KRAS* gene accounts for 95% of pancreatic, 55% of thyroid, 35% of colorectal and 35% of lung carcinomas[3]. By looking at a person's genome, a diagnosis can be rendered quickly and accurately, leading to a greater likelihood of a successful treatment. Unfortunately, while this can be done for small fragments of a person's genome, it is far more expensive to sequence a patient's DNA in its entirety.

As an example, the HiSeq X series from Illumina can be considered [4]. This instrument is the newest of the next-generation DNA sequencing platforms, and is arguably the most cutting edge to date. While it has not yet been thoroughly tested in the field, the specifications of the HiSeq X claim it can sequence the entire genome of a person for less than $1000 [4]. This is a significant step towards creating a cost-effective sequencing device, although the present price tag for 10 machines is listed at "at least $10 million", which is prohibitively high for many users [4]. Importantly, the time required to process a single genome is not trivial; roughly 5 genomes can be processed per day when the instrument is running at maximum capacity. This is exciting in the sense that timescales are improving from older methods, however to reach the volume of samples required to recoup the cost of the machine is quite high. If we assume 10 machines are obtained for $1 million dollars apiece and operated at 85% capacity every day, it would take 4 years for the cost to average out to ~$995 per genome [4]. Additionally, while the HiSeq X is a state-of-the art instrument, it is a large piece of equipment which requires long sample processing time with highly trained staff to operate them. Furthermore, these instruments would likely require a designated centralized laboratory. Unfortunately, all of these accommodations add complexity and cost to the process. While the HiSeq X is poised to become the top sequencer available, improvements must be made in next generation sequencing platforms in order for personalized medicine to really take off. One of the frontrunners at this point is nanopore technology, particularly solid-state nanopores due to their robustness and tunability [5].

Solid-state nanopores are an attractive alternative to traditional sequencing platforms for a number of reasons. First, there is the simplicity of the experiments. With solid-state

nanopores, in contrast to many other sequencing methods, there is often no need to rely on fluorescent tags or the use of enzymes. Instead, the molecule of interest can be interrogated in its native state, with the pH, molarity and aqueousness of the environment all being tuneable. This not only gives rise to simple experiments, but also gives the researcher the flexibility to either keep molecules in their expected conformation, or probe chemical bonds through the use of different solvents [6]. Second, while other cutting edge platforms tend to have short read lengths (typically on the order of 150 bp [7]), nanopore based platforms have been utilized in conjunction with DNA fragments in the ~50 kbp range, but theoretically could be used with fragments of any length [8]. Through the use of these long reads, it is conceivable that there would no longer be the need for amplification of the DNA through polymerase chain reaction (PCR), significantly decreasing the complexity and the time required to operate the system. Third, solid-state nanopores have the potential to investigate more than just the DNA, and delve into epigenetics. For instance, methylation has been under scrutiny of late, and it has been shown that certain methylation conditions can be indicative of susceptibility to cancer [9]. Solid-state nanopores, which have already demonstrated the capability of identifying methylated regions of DNA [10], could perform both a diagnostic assay to identify methylation centers or other epigenetic factors, while also providing the option of DNA sequencing. Finally, and perhaps most importantly, solid-state nanopores offer the potential of point-of-care testing that many other technologies cannot provide. Due to their small size and ease of use, it is possible that solid-state nanopores could be utilized at the bedside of a patient by a nurse or doctor. In fact one device, a biological nanopore-based system called ‘MinION’ by Oxford Nanopore, has already launched an early-access program based on this principle. The MinION device is small enough to fit in the palm of a person’s hand, and is

operated by plugging it in to a computer's USB port. With the help of custom software, it has the ability to perform typical nanopore experiments and produce data in real time [11].

Solid-state nanopores are presently one of the most promising platforms to provide personalized medicine in a rapid and cost effective way. The purpose of my work was to tackle some of the potential roadblocks that must be overcome for solid-state nanopores to become a serious contender in the medical field.

1.1 Typical Solid-State Nanopore Setup

Irrespective of whether or not solid-state nanopores become the next big sequencing platform, they are one of the simplest ways to analyze a single molecule with high sensitivity.

A typical nanopore experiment consists of a thin insulating membrane containing a solitary nanopore, sandwiched between two electrolyte-containing fluidic reservoirs. Gaskets, typically made out of some flexible material, are used to ensure the nanopore is the only fluidic path between the two reservoirs. The fluidic reservoirs themselves are milled in a durable and inert material, typically PEEK (Polyether ether ketone) or Teflon, which applies pressure to both gaskets, compressing them against the nanopore chip and eliminating the possibility of leaks. Finally, non-polarizable electrodes are placed in each of the fluidic reservoirs, and are used to apply a voltage across the membrane. Typically the electrodes are made of silver chloride, allowing for the following reversible redox reaction to occur:

$$Ag(s) + Cl^- \rightleftharpoons AgCl(s) + e^- \qquad [1.1]$$

When an electric field is applied across the membrane, a steady stream of ions is driven through the nanopore which results in a small but measurable current. The current is directly proportional to the nanopore size, which allows for extremely precise measurements to be made. This will discussed further in Section 1.2.

The overall design, minus the electrodes for clarity, is presented in Figure 1.2. The extra well in the half cell presented in the Figure is not connected to the electrolyte-based circuit, but is instead used to keep evaporation of water from the electrolyte to a minimum.

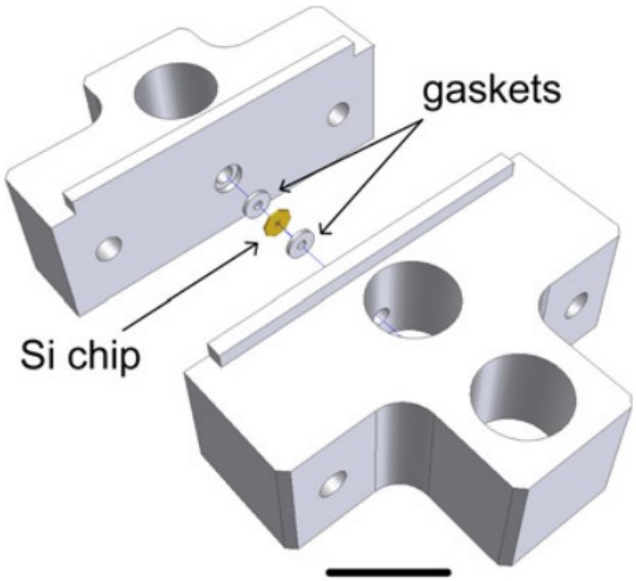

Figure 1.2. An exploded view of a typical cell assembly. Two half cells are shown in white with a reservoir in each that allows fluidic access to the Si chip. The extra well on the larger half-cell is filled with water to minimize the effect of evaporation. The gaskets are made of silicone elastomer, and form a liquid tight seal around the Si chip. The scale bar is 1 cm. © IOP Publishing. Reproduced with permission. All rights reserved. [108]

Alternatively, the nanopore system can be modeled as a simple circuit, as is represented in Figure 1.3. This allows for the utilization of electronics-based calculations to determine relevant information, such as the size of the nanopore.

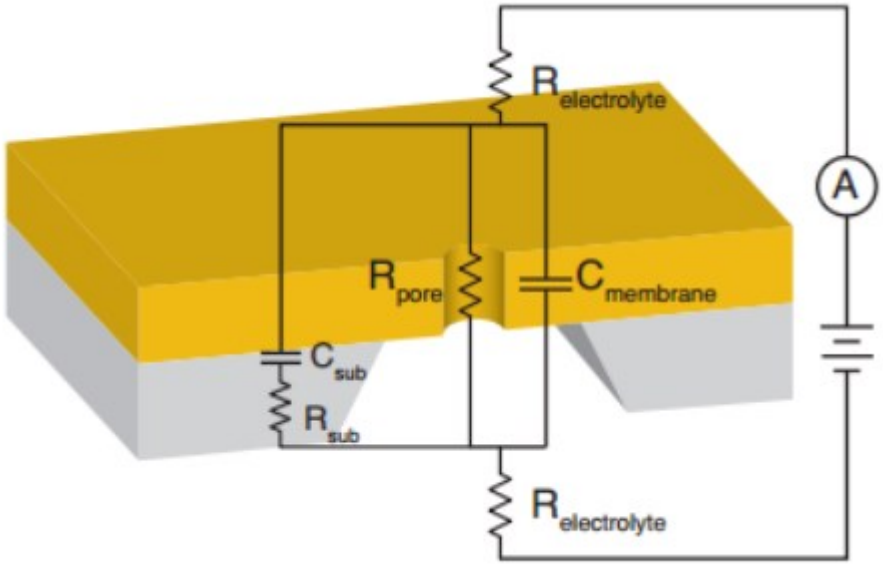

Figure 1.3. Schematic of a typical nanopore in a thin membrane, overlaid with the corresponding circuit components. Reprinted from [109], with permission from Elsevier.

1.2 Conductance of a Nanopore

From Figure 1.3, it is evident that the nanopore system can be represented by a rather simple circuit. Importantly, solid-state nanopores are typically run at high salt concentrations, which causes $R_{electrolyte}$ (the resistance due to the electrolyte) to become negligible compared to R_{pore} (the resistance due to the pore), and all of the voltage drop can be assumed to be entirely across the nanopore. This idea is useful, as it means that an I-V curve obtained by a voltage sweep can measure R_{pore}, which is directly proportional to the size of the nanopore. However, it is not just

the nanopore size that determines R_{pore}; as Figure 1.4 demonstrates, R_{pore} can be broken down into three components, namely:

1. Resistance due to geometry (length and diameter)
2. Access resistance
3. Resistance due to the surface charge

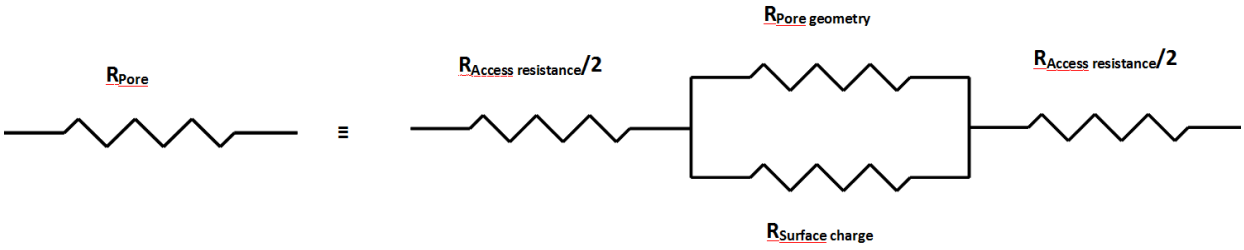

Figure 1.4. Circuit diagram of the components which make up R_{pore}.

1.2.1 Resistance Due to the Geometry

For simplicity, nanopores are generally assumed to be cylindrical. Based on this assumption, and using the basic equation for resistance between two electrodes in solution, the conductance for a nanopore can be obtained:

$$G = \sigma \frac{\pi {d_{pore}}^2}{4L_{pore}} \qquad [1.2]$$

where G is the conductance of the nanopore, σ is the conductivity of the solution, d_{pore} is the diameter of the nanopore and L_{pore} is the length of the nanopore.

Under normal experimental conditions, this geometry term dominates the conductance of the nanopore.

1.2.2 Access Resistance

The access resistance term describes a hemispherical volume just outside of the nanopore on either side. In this region, the voltage decays from the value at the mouth of the nanopore to the value of the electrode on that side of the membrane. The radius of this region is usually on the order of nanometers or micrometers, depending on the conductivity of the solution and the diameter of the nanopore.

In essence, the access resistance term is measuring the resistance from a planar disc (the mouth of the nanopore) to the electrode, which is assumed to be very far away. It turns out the resistance between the two 'electrodes' is dominated by the narrow region where the current approaches the electrodes [12]. While the derivation is beyond the scope of this thesis, the result is the generation of the following equation [12,13]:

$$G_{acc} = 2\sigma d_{pore} \qquad [1.3]$$

Importantly, while this represents one of the sides of the nanopore, there will be an access region present on both sides of the membrane, each contributing equally to the resistance. Therefore, when taken together, the overall conductance due to the access resistance of the nanopore system would drop the coefficient of 2 from Equation 1.3.

1.2.3 Resistance Due to the Surface Charge

Finally, there is the surface charge of the walls of the inside of nanopore contributing to the change in the conductance. This comes about by the fact that silicon nitride membranes (common for solid-state nanopore work) tend to be negatively charged under experimental conditions, thus the walls of the nanopore can also be negatively charged. This charge is shielded by mobile positive charge carriers (e.g. K^+ or Li^+), which form an electrostatic double layer. Since this double layer necessitates that a greater number of ions are found within the nanopore than would be if no charge was found on the wall of the nanopore, this increases the conductance of the nanopore system. This is the only term that does not depend on the conductivity of the solution, and the equation for this term is given as [14,15]:

$$G_{surface} = \frac{\mu_* \pi d_{pore} \rho}{L_{pore}} \qquad [1.4]$$

where μ_* is the solution mobility of the counterion that is adsorbed onto the charged surface of the pore, and ρ is the surface charge density of the walls of the nanopore.

The overall equation for the conductance of a nanopore of a given length and diameter can be written as follows:

$$G = \sigma \left(\frac{4L_{pore}}{\pi {d_{pore}}^2} + \frac{1}{d_{pore}} \right)^{-1} + \frac{\mu_* \pi d_{pore} \rho}{L_{pore}} \qquad [1.5]$$

Despite the knowledge that the conductance can be affected by surface charge, it is not used for the remainder of this thesis. There are two main reasons for this: first, it is difficult to obtain an accurate measurement for either the mobility of the counter ions adsorbed onto the charged surface of the pore or the surface charge on the pore walls and, second, is that the impact on

conductance in high molar conditions (≥ 1M) is negligible compared to the other two previously mentioned conductance terms. As a result, the equation simplifies to:

$$G \cong \sigma\left(\frac{4L_{pore}}{\pi {d_{pore}}^2} + \frac{1}{d_{pore}}\right)^{-1} \qquad [1.6]$$

1.3 Size Estimation

For many practical nanopore based single molecule experiments an estimate of the nanopore size is required. For instance, the pore must be larger than the molecule that the researcher is trying to pass, but not so large as to drown out the signal. Using Equation 1.6 and solving for d_{pore}, we obtain the following equation:

$$d_{pore} = \frac{G}{2\sigma}\left(1 + \sqrt{1 + \frac{16\sigma L}{\pi G}}\right) \qquad [1.7]$$

By extracting the slope of an *I-V* curve obtained with a nanopore, the conductance *G* (G = ΔI/ΔV) is obtained, as shown in Figure 1.5.

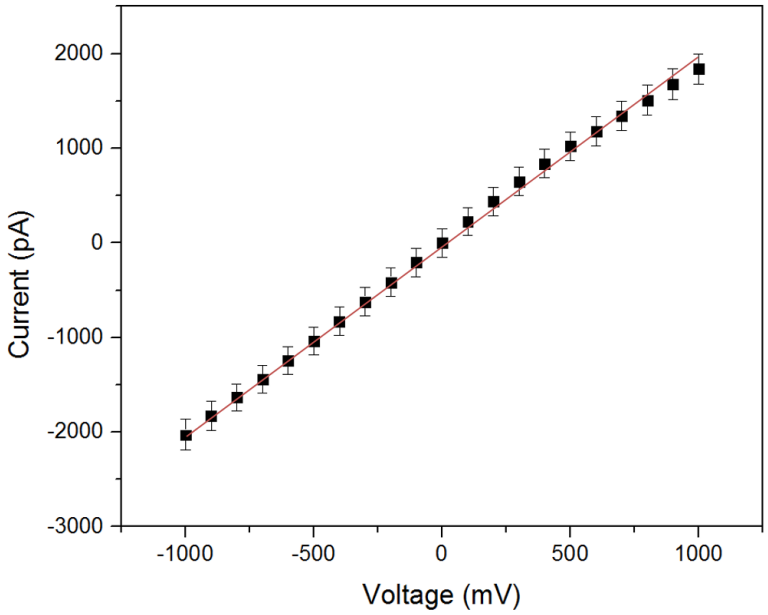

Figure 1.5. Plot of typical *IV* curve for a 10 nm thick membrane containing a nanopore submerged in 1 M KCl. Based on the data shown, the size was estimated to be 1.7 ± 0.1 nm in diameter, depending on the polarity of voltage due to slight rectification.

1.4 Nanopore Fabrication

1.4.1 TEM

Traditionally, nanopore fabrication has been done through the use of an ion beam, typically a transmission electron microscope (TEM) [16]. However, the creation of nanopores using a TEM is a complex method which includes the use of a high vacuum inside the TEM chamber (10^{-5} Pa), focusing the electron beam on the membrane, and drilling the nanopore in such a way as to ensure pore formation by sputtering. The difficulty arises from the necessity to create a pore small enough for use by manually defocusing the beam once flickers on a fluorescent screen are observed by eye. This is an expensive and time consuming process, as even experienced users are only able to make roughly ~4 pores per hour [17]. Additionally,

the yield of making pores of the correct size that are suitable for biological detection is generally < 30% [18,19]. One of the biggest drawbacks of making nanopores using a TEM is the sheer cost of the TEM itself. They can easily cost a million dollars, which is simply prohibitive for many researchers, and makes scaling nanopore based technology up to an industrial level very difficult, if not impossible.

After nanopore drilling, the chip itself needs to be cleaned in order to remove any carbonaceous residue left over from the TEM vacuum. Typically this is achieved by performing a piranha clean on the chip, which employs a sulfuric acid and hydrogen peroxide solution [20]. Unfortunately, this harsh treatment frequently leads to enlargement of the nanopore and thus negates the benefits of being able to visually inspect the nanopore with the TEM to confirm nanopore size and geometry [17,19]. Additionally, due to this unwanted enlargement through cleaning, it is difficult to create the sub-3 nm pores required for analysis of ssDNA sequence identification applications [17].

In summary, while TEM drilling to form nanopores has been the benchmark of solid-state nanopore fabrication for many years, it is far from ideal. A different method for pore formation should be used if solid-state nanopores are to be utilized on a commercial scale and by a wider research community.

1.4.2 Controlled Dielectric Breakdown

Recently, a breakthrough was achieved in the Tabard-Cossa lab which makes the entire process much simpler and less expensive [16]. This novel technique relies upon the phenomenon of dielectric breakdown of a thin SiN_x membrane.

In this technique, rather than submerging a pre-formed nanopore on an insulating membrane (supported by a silicon chip) into an electrolytic solution, a blank insulating membrane (supported by a silicon chip) is submerged. The electrolytic solution is typically 1M KCl pH 8, which does not etch SiN, while the chip itself is a silicon wafer with a SiN_X layer on one side. Once submerged, an Ag/AgCl electrode is placed on either side of the membrane in order to produce a voltage across it, with the thickness of the membrane dictating the magnitude of the applied electric field. For membranes of ~10 nm in thickness, 8V is a typical value, whereas ~30 nm thick membranes require roughly 14V. At this field strength (>0.5V/nm), sustained leakage current is observed and can be monitored in real time as it passes through the dielectric membrane. Despite the leakage current passing through the membrane, there is still no fluidic path connecting the two sides of the membrane, and it remains insulating at low fields. It is believed that this leakage current arises from redox reactions occurring on both sides of the membrane simultaneously, with one side donating electrons and the other accepting them. Inside the membrane, it is believed the electrons undergo trap-assisted tunneling, however at present, the exact redox reactions occurring are unknown. Considering the potential applied across the membrane is above the overpotential of many reactions, it is possible there are many reactions occurring simultaneously.

As these traps begin to accumulate, a localized conductive path is created randomly on the membrane. This leads to a greater number of electrons moving through this particular path, and an avalanche effect is realized. Eventually the material fails and is removed, leaving behind a solitary nanopore. This process is demonstrated in Figure 1.6.

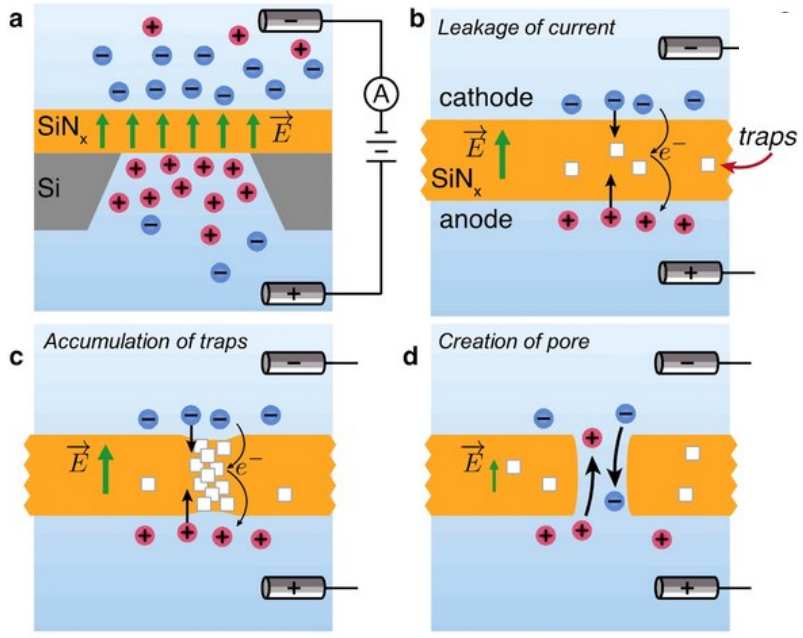

Figure 1.6. Schematic overview of nanopore formation by controlled dielectric breakdown. a) An electric field is applied across the membrane, which causes an electric field within the membrane itself. b) Charges produced at the surface of the membrane undergo trap-assisted tunneling through the membrane. c) A localized conductive path forms, and d) a pore forms. Reprinted from [16].

Importantly, throughout this process we are able to monitor the leakage current, and this discrete breakdown event is marked by a large increase in the current as the newly formed nanopore connects the two reservoirs with conductive solution. Conveniently, a computer program can be used to interrupt the voltage immediately after the current reaches a certain threshold. This immediate voltage shutoff is important to maintain a small pore size, as a large voltage applied to an existing nanopore tends to grow the pore, and it can easily reach sizes that are too large to be useful [20].

Figure 1.7 shows a typical nanopore fabrication event for a 30 nm thick membrane. As shown in red, -14 V is applied across the membrane at time zero. A large spike in current, shown in blue, occurs due to the capacitance of the device. After the capacitance-induced current has decayed (which can take ~1-2 s), a stable leakage current is measured, which slowly decays. Eventually, as seen at ~16 000 s, the current increases abruptly, indicating a pore has formed, and the voltage is cut off. This pore took a very long time to form, however this was by design, and for reasons outside of the scope of this thesis. It is possible to reliably form experimentally relevant nanopores in <10 min.

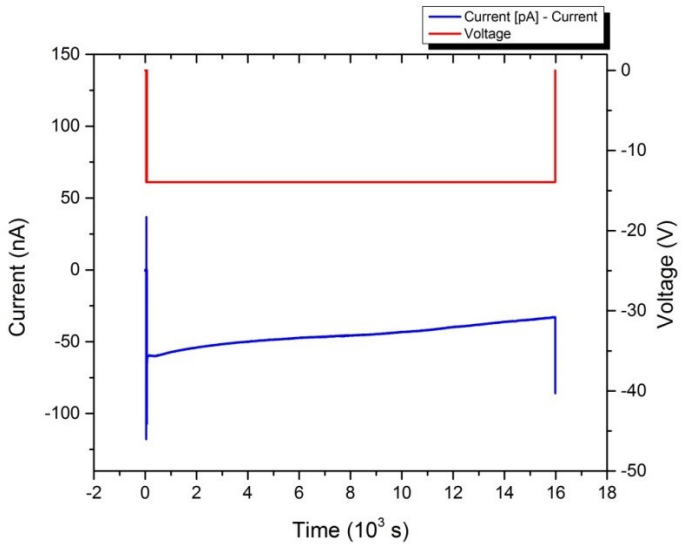

Figure 1.7.Trace of typical nanopore fabcrication event using a 30 nm thick SiNx membrane, where current and voltage are denoted by blue and red, respectively. The onset of the voltage across the membrane produces the first large current spike. After it decays, the current becomes stable until breakdown occurs, marked by the second current spike.

Using this technique, nanopore sizes previously unattainable can be made with relative ease. It has been demonstrated that low-noise pores <2 nm in diameter can be created reliably, laying the groundwork for more single-stranded DNA experiments, something that is

necessary in order to continue to progress in the field of nanopore-based medical diagnostics. There are, however, hurdles that still loom large. One of the biggest challenges that must be overcome is the rapidity with which biomolecules translocate through solid-state nanopores [21,22].

1.5 Solid-State Nanopores as Molecule Sensors

One of the benefits of solid-state nanopore platforms for single molecule analysis is their simplicity. To perform an experiment to detect a biomolecule of interest, the user only has to inject the unlabelled sample into one of the two fluidic reservoirs. In order for the molecule to translocate from one side of the membrane to the other, it must be 'captured' by the nanopore. This occurs when the molecule crosses what is termed the *capture radius*, a hypothetical hemisphere of radius r* outside of the nanopore. Here, the electric field is strong enough that it dominates over Brownian motion, and essentially all biological molecules that diffuse into this capture radius translocate through the nanopore. The equation for the determination of this radius is presented in Equation 1.8 [23]:

$$r^* = \frac{{d_{pore}}^2 \mu_{DNA}}{8 L_{pore} D} \Delta V \qquad [1.8]$$

Where μ_{DNA} is the electrophoretic mobility of DNA, and D is the diffusion constant. Generally, this radius is ~2 μm for a standard nanopore experiment.

Once the molecule has entered the sensing region of the nanopore (which, as mentioned in Section 1.2.2, may extend into the bulk solution), its presence begins to affect the conductance

of the nanopore system. The resulting change in current can be measured, and it is this electrical signal that is the basis for single molecule analysis in a solid-state nanopore device.

The origin of this conductance change is rooted in the fact that a molecule residing in the sensing region of a nanopore will occupy some volume that would otherwise be filled with mobile ions. Therefore, if the molecule introduces a different charge density into the sensing region than the bulk electrolyte solution, a change in conductance will occur. Importantly, many biomolecules are highly charged, so special attention must be paid to ensure the charge density of the molecule in question (and its associated counter ions) does not equal the charge density of the bulk solution. In such a case, the translocating biomolecule will introduce no net change in conductance, and no change in current can be observed [14]. For this reason, it is generally desirable to maintain the bulk charge density as dissimilar to the molecule of interest as possible. Interestingly, if a researcher chooses to keep the charge density of the bulk solution lower than that of the molecule, the conductance will increase when the molecule is inside the pore, resulting in an increase in current. This is generally not the method of choice as it results in weak signals, but is sometimes necessary for purposes where weak non-covalent intermolecular interactions are present, such as protein binding. Typically high molar salts are used, as much stronger signals can easily be achieved due to the difference in charge density between the bulk and the biomolecule. In the case of DNA-based experiments performed in KCl, the crossover point from current enhancement to current reduction is 370 ± 40 mM at pH 7.5, for a silicon nitride nanopore with typical thickness and diameter [14]. Therefore, in order to ensure an observable signal from each passing DNA molecule, a large bulk conductivity is desirable, as seen in Equation 1.9.

1.6 Translocation

Once a molecule is inside the nanopore, the current between the two electrodes is read and interpreted. In order to be fully confident in the measurements, it is useful to compare the change in current (ΔI) that arises from a DNA translocation to the predicted change in current $\Delta I_{theoretical}$, derived from a simple ohmic-based model. This step provides support to the fact that the signal originates from a fully translocated molecule and is not a collision event, or some form of contamination or noise. $\Delta I_{theoretical}$ is obtained in a similar fashion to Equation 1.2, and can be written:

$$\Delta I = \sigma \frac{\pi {d_{DNA}}^2}{4L_{pore}} * V \qquad [1.9]$$

where V is the applied voltage, and d_{DNA} now refers to the diameter of DNA, which reflects the total volume of ions that are excluded from the pore as a result of the biomolecule presence. In this case, we assume that the net charge density of DNA is insignificant compared to that of the surrounding bulk solution that it is displacing. While this is not valid for low molarity salt solutions as argued above, it is an acceptable approximation for the experiments performed within this thesis, which use either 1M KCl or 3.6M LiCl.

It should be noted that the change in current is dependent on the square of the diameter, which allows for highly precise radial measurements. This radial resolution is one of the greatest features of nanopores, and gives rise to the possibility that they could be used to sequence DNA based on the physical size difference of each base. Recently the potential of nanopores was put on display, as a solid state nanopore was used to differentiate short homopolyers of

ssDNA, which represents a significant step towards sequencing technology. This is presented in Figure 1.8.

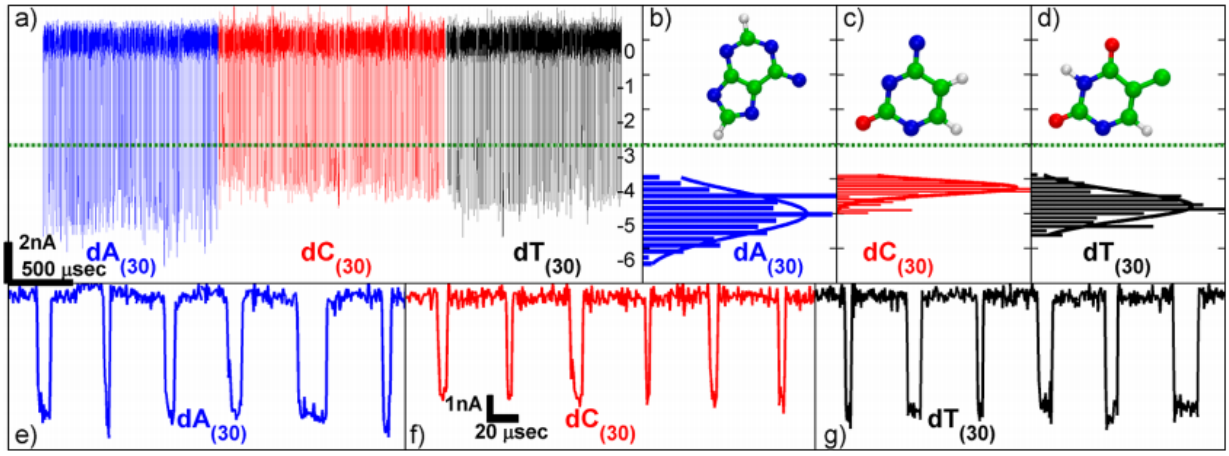

Figure 1.8. Results from Venta, K. *et al*. showing the differentiation of short (30-nt) single stranded DNA homopolymers by the use of solid-state nanopores. a) depicts individual events that have been concatenated for polyA, polyC and polyT fragments of ssDNA. The dashed line represents the threshold for defining events. b), c) and d) Normalized histogram of event depths for polyA, polyC and polyT, respectively. e),f) and g) selected events from the current trace for each DNA fragment. Reprinted from [110]. Copyright 2013 American Chemical Society.

While the results demonstrated in Figure 1.8 are very exciting, the current traces in e-g) show that many of the translocating molecules move at a rate >1 nt/µs. At that speed, molecules as a whole can be poorly resolved, let alone individual bases. This issue of poor temporal resolution is representative of one of the largest hurdles that must be overcome to enable solid-state nanopores to be truly useful in health science applications.

1.7 Rapidity of DNA Translocation

One of the greatest issues that must be overcome before solid-state nanopores can exist as a next generation sequencing platform is that of translocation speed. It is true that some assays are already possible using solid-state nanopores, like the estimation of methylation [10], however the ultimate goal of solid-state nanopores is to perform rapid and cost efficient DNA sequencing. To do this, nanopores must be capable of not just differentiating homopolymers as shown above, but individual bases on a DNA molecule [21,22,24]. It can be argued that complex statistical analysis could allow for sequencing without the need for obtaining a unique current signature from each base, but present technology is still far away from where statistical methods become relevant. Thus the problem remains, and a method for either slowing down DNA translocation, or increasing our instrumentation bandwidth needs to be developed in order to overcome the background noise and signals from adjacent bases [22,25]. To illustrate this point, a standard nanopore experiment can be considered. When a 5-kbp dsDNA molecule is translocated from one side of the membrane to the other under typical experimental conditions (1M KCl, 600 mV applied voltage), essentially all of the molecules translocate in less than 100 μs (Figure 1.9). Taken together, this means that the minimum speed with which any given molecule is traveling is 50 bp/μs. Our hardware, on the other hand, has an effective bandwidth of ~50 kHz, meaning the rate of translocation needs to be ≤0.05 bp/μs in order to obtain a meaningful signal for an individual base. Clearly, improvements are necessary before sequence data can be acquired from translocation events.

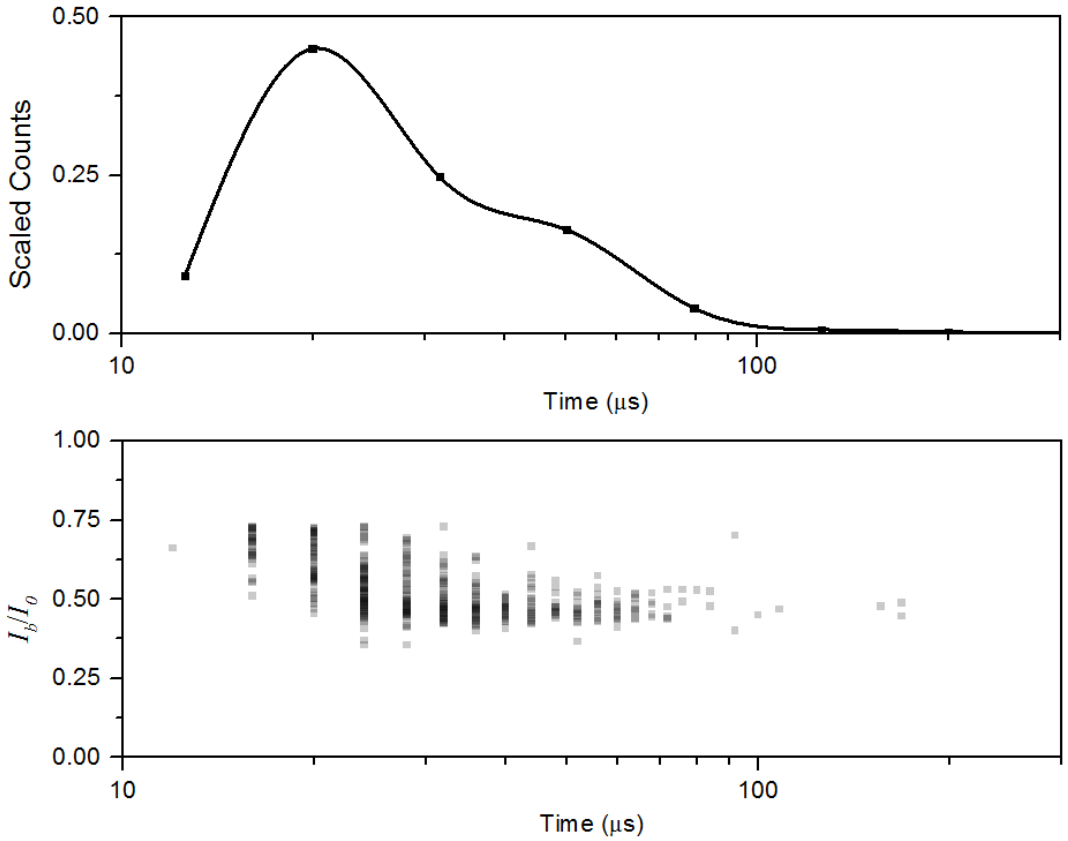

Figure 1.9. a) Histogram of translocation times normalized to 1, and b) the percent of current passed during individual translocations plotted against the translocation time during a typical solid-state nanopore experiment performed with 5kbp DNA fragments in 1M KCl and operated at 600 mV. The SiNx membrane is 10 nm thick and the pore is ~4 nm in diameter. While it appears that the molecules traversing the pore more quickly have a smaller blockage depth, this is a result of the bandwidth of the Axopatch 200B.

It may be tempting to reduce the voltage in order to reduce the electric field acting on the translocating molecule and therefore slow it down, however this approach introduces a new set of problems [26]. First, the reduction in the applied voltage decreases the current passing through the nanopore, which reduces the strength of the signal (see Equation 1.9). Second, with a reduced applied force the Brownian motion becomes more prominent and causes the molecule to move unpredictably leading to backtracking, or skipping ahead of important read-sites of the molecule [26]. Figure 1.10 demonstrates this issue, where a simulation of an ideal detector reading ssDNA is compared without Brownian motion, when the ratio of thermal

noise to work done by the driving force is similar to that of typical nanopore experiments (k_BT/Fa ≈ 5, where a is the distance between successive nucleotides), and finally when the ratio of thermal noise to work done by the driving force is reduced to 0.1 by increasing the driving force by a factor of 50 [26]. It is evident from the data that a voltage strong enough to overcome thermal fluctuations is desirable for clean and less error-prone reading.

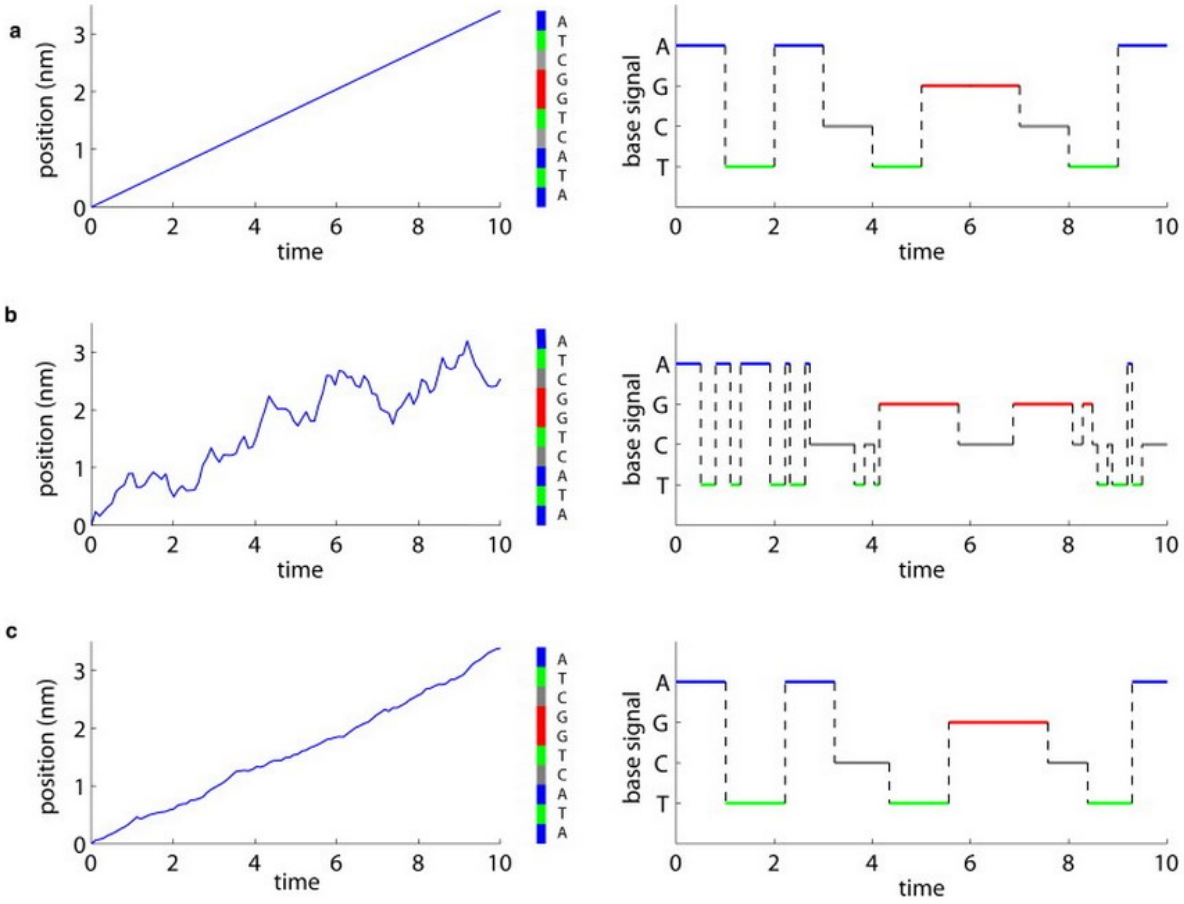

Figure 1.10. A simulation of a 10-base ssDNA strand passing through a detector with single base resolution under various conditions. a) No Brownian motion is present (ratio of k_BT/Fa = 0), and the molecule passes through the detector with a constant velocity, and the signal recorded is clear. b) Ratio of k_BT/Fa ≈ 5, similar to typical nanopore technologies, leading to an error-prone signal. c) Ratio of k_BT/Fa ≈ 0.1 by increasing the driving force by a factor of 50, suppressing the motion due to thermal fluctuations and producing a clean signal. It should be noted that the time axis is normalized to the average base translocation time [26].

In summary, the velocity with which molecules traverse solid-state nanopores is problematic for many practical applications. Ideally, a voltage could be applied that would overcome the issue of Brownian motion while simultaneously reducing the velocity to a level where each nucleotide on a ssDNA molecule would be sampled for ≥20 μs. Importantly, advances have been made in increasing the bandwidth of detection instruments to the 1 to 5 MHz range [27,28] which reduce the necessary dwell time of each individual nucleotide, however molecules are still translocating over an order of magnitude too quickly for complete nanopore-based DNA sequencing to become a reality [27]. In order to address this issue, researchers have turned their attention to three basic components of the nanopore system – the environment, the molecule of interest, and the nanopore itself.

1.7.1 The Environment

In terms of the environment surrounding the nanopore, both biological and solid-state nanopore researchers have experimented with methods to slow the movement of the electrolytic solution. Specifically, reducing solvent temperature [29,30] and increasing viscosity [31–33] both showed a reduction in translocation speed when passing DNA molecules. Additionally, solid-state researchers have explored the use of alternate salts [14,34] and the introduction of a salt concentration gradient [35,36] or counter pressure [37,38], achieving close to 10-fold translocation rate reductions by each of these means [38]. Unfortunately, biological pores are often unable to handle a departure from physiological conditions, and thus varying the pH or pressure is not possible.

While these methods have been successful at reducing the rate at which DNA translocates through nanopores, they are not without their price. As altering the environment typically involves altering the surroundings of the DNA as well as the ions, the entire solution is slowed, not simply the DNA. The crux of this is that DNA will move slower not only in the nanopore, but also outside of it, limiting the capture rate to a much lower value. Additionally, and potentially more detrimental, is that Equation 1.9 suggests that these methods will negatively impact the signal to noise ratio due to the change in current scaling linearly with the conductivity of the solution. For example, if a solution with greater viscosity is used in the setup, ions will move slower in the solution, and therefore the solution has a lower conductivity, and thus a smaller signal.

1.7.2 The Molecule of Interest

Efforts to slow translocation have also focused on modifying attributes of the molecules of interest, employing molecular motors or tethering them to mechanical probes. For biological nanopores, the addition of bulky tags to the analyte was found to diminish translocation speed [39] while enzymes [25] permitted ratcheting (also called processive translocation [40–43]) as well as a closer look at DNA-enzyme interactions [44]. In fact, combining enzymes with an MspA nanopore [45] enabled single-nucleotide resolution [46] of ssDNA strands. Combining DNA hairpins [47–50] or avidin-bound ssDNA [51–53] with biological nanopores has facilitated slower translocation and repeated interrogation of the same molecule by physically blocking the molecule from completing its passage through the nanopore. Similar results have been achieved through the incorporation of optical tweezers [54,55],

magnetic tweezers [56], or AFM tips [57] in solid-state nanopore experiments. While these modifications to the analyte have slowed translocation rates significantly [57], it should be noted that a significant selling point for a nanopore-based system is high-throughput and scalability to obtain rapid results at low cost. Many of these approaches inherently add layers of complexity, while the ideal nanopore device would not require such modifications [21].

1.7.3 The Nanopore

A final route to slowing translocations has involved modification of the nanopore itself. For example, modifications to solid-state nanopores have included adjusting the nanopore diameter to increase friction [58–60], modulating the nanopore surface charge with laser light [61], functionalizing the nanopore with hydrogen-bonding molecules [62] or coating it with a lipid bilayer [63], and altering the properties of a pH-responsive organic nanopore coating [64]. Additional methods have been proposed, including local heating of a gold layer surrounding the nanopore to stretch the DNA [65,66] and ratcheting of nucleotide strands through introduction of a third electrode [67,68]. In fact, researchers have investigated a three-terminal system, or field effect nanofluidic transistor, which would alter the electric field profile in the nanopore [69–71] and modulate its surface charge [72–75]. Base-by-base ratcheting using electrostatic traps in a DNA transistor has yet to be achieved, but nanopore modifications have already reduced translocation speeds by up to an order of magnitude for ssDNA [62,73].

In an effort to continue the push of solid-state nanopores towards DNA sequencing while avoiding the pitfalls inherent with changing the environment and/or the molecule itself, it was determined that focusing on altering the pore was the best choice.

1.8 Motivation and Design

In order to address the issue of DNA's prohibitively fast translocation through solid-state nanopores, I first determined that the best approach would be to leave the *cis* side unaltered. My reasoning centered on the capture rate of DNA; if I were to design a system that would limit the DNA's motion at all points within a given radius near the nanopore, the capture rate would be significantly impacted, leaving us with fewer results. This is less than desirable, as many nanopore-based methods require a statistically relevant number of single-molecule translocation events (e.g. hundreds) to differentiate two similar molecules.

My attention was therefore turned towards altering the *trans* side of the membrane, as there was no reason to suspect that it would hinder the capture of DNA molecules on the *cis* side. This lead to the thinking that by rendering it more difficult for the molecule to move into the *trans* side of the nanopore, I could potentially reduce it's speed without hurting capture rate. To test this, I decided to utilize a gel that would be placed on the *trans* side which would interact with the DNA as it translocated through the nanopore, slowing it down. Importantly, the gel is completely permable to ions and thus does not impact the signal in any meaningful way.

Specifically, I turned to the use of two well-known and well-characterized gels, agarose and polyacrylamide, both of which are used regularly in order to sieve DNA and proteins. The behaviour of DNA within a gel can be complex, and is discussed in greater detail in Section 1.10.

1.9 Reviewing Previous Gel-Nanopore Work

Concurrent work has been done on the basis of using a gel-interfaced solid-state nanopore to slow down DNA[76], which is important to mention. In this work, the authors placed what they termed a nanofiber mesh on to the *cis* side of the membrane, which the DNA would travel through before going into the nanopore, and finally exiting into free solution onto the *trans* side, as shown in Figure 1.11.

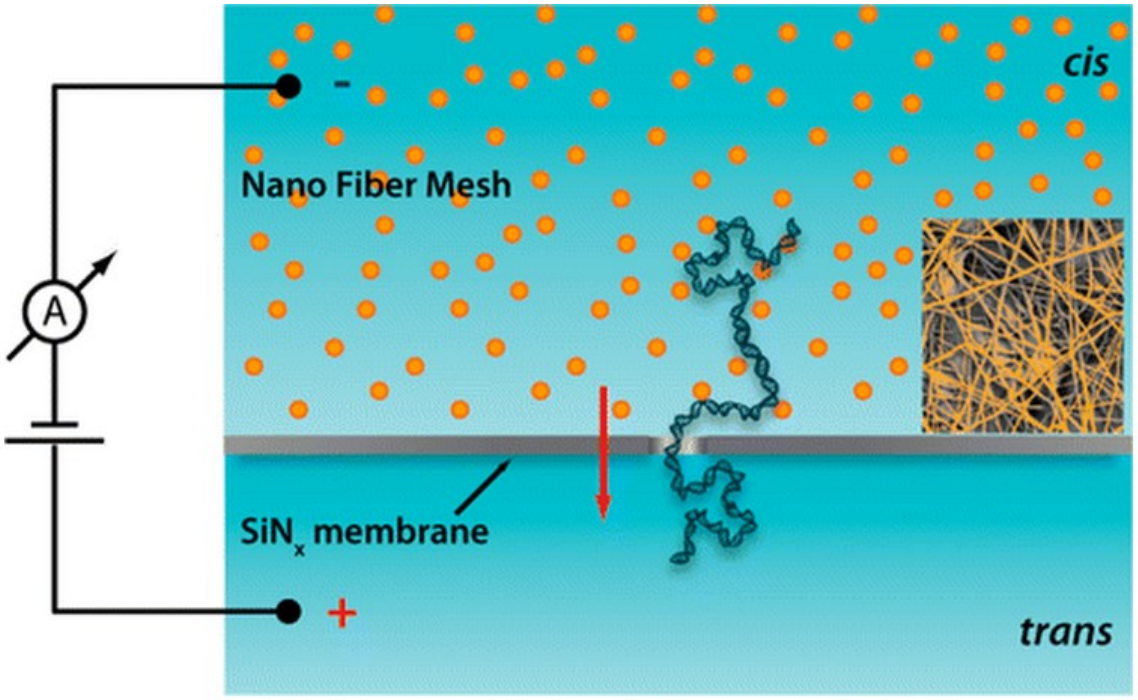

Figure 1.11. Schematic of DNA translocating through a nanopore interfaced with a nano fiber mesh coating the *cis* side. Inset is a SEM image of a nanofiber mesh on a nanopore chip.

This concurrent work is interesting, and differs from ours in some important ways. First, and most obviously, the mesh is on the opposite side of the membrane. I chose not to pursue this avenue of research because the DNA must leave the free solution and enter into the gel in order to reach the nanopore, something that introduces a large entropic barrier. Instead, the molecules will tend to stay in the free solution if there is no applied force. The Squires *et al.* paper uses an intelligently designed technique to overcome this issue by electrospinning a very thin mesh (on the order of microns) on the membrane, allowing for a weak electric field to extend from the nanopore into the free solution, and thus reducing the entropic barrier such that some molecules may overcome it and enter into the gel fibers, as shown in Figure 1.11. This is a unique way of solving the issue, however this *cis*-side mesh adds an undesirable reduction in capture rate, which I was looking to avoid. Additionally, the polymer used as the

nano-mesh was custom-made (PGC-18), and required in excess of 56 hours for a chip to be prepared [76], increasing experimental complexity. Importantly, and in contrast to my work, this custom-made polymer is not as well characterized as either agarose or polyacrylamide, meaning interpreting the results was a challenging task.

Again, while I wanted to avoid a system as complex as the one developed by Squires *et al.*, their work is interesting, and opens the door for many new methods involving a thin mesh on the *cis* side of nanopore membrane as a means of slowing DNA passage.

1.10 Behaviour of DNA

In order to fully understand and appreciate the aim and results of utilizing a gel to slow down DNA passing through a solid-state nanopore, it is imperative to understand the behaviour of DNA both in free solution and in gel.

1.10.1 DNA in Free Solution

In free solution, the highly negatively charged DNA molecule will perturb the ions in the solution, and these ions will move to shield the charges of the DNA, a phenomenon termed Manning condensation [77]. This results in two layers of charged ions forming what constitutes the electric double layer, or EDL, as depicted schematically in Figure 1.12. The characteristic length scale, the Debye length (l_D), is established by the interplay between drift and diffusion of the ions, and can be calculated as $l_D = 0.303/\sqrt{c}$, where c is the molar

concentration of the monovalent ion [78] (typically on the scale of 2Å for nanopore experiments). The innermost region is comprised exclusively of counter ions (in the case of DNA, positive ions) which adsorb to the surface of the charged particle, and is termed the Stern layer. The second layer is called the shear layer, and is more loosely associated with the particle. The shear layer is made up of ions bound to the particle through the Coulomb force that help screen out any residual charge from either the solid or the Stern layer, and therefore can contain both negative and positive ions. As the distance from the charged particle increases, the charge density decreases. Importantly, there is some boundary that is defined as the no-slip boundary, beyond which the ions can be moved away from the particle with some tangential force, while inside of this boundary the ions are more or less fixed. The no-slip boundary is represented by ζ, and separates the shear layer and the diffusive layer. Not depicted is the Bjerrum length, which is defined as the distance between two charged bodies where the electrostatic interactions is comparable to the thermal energy [79].

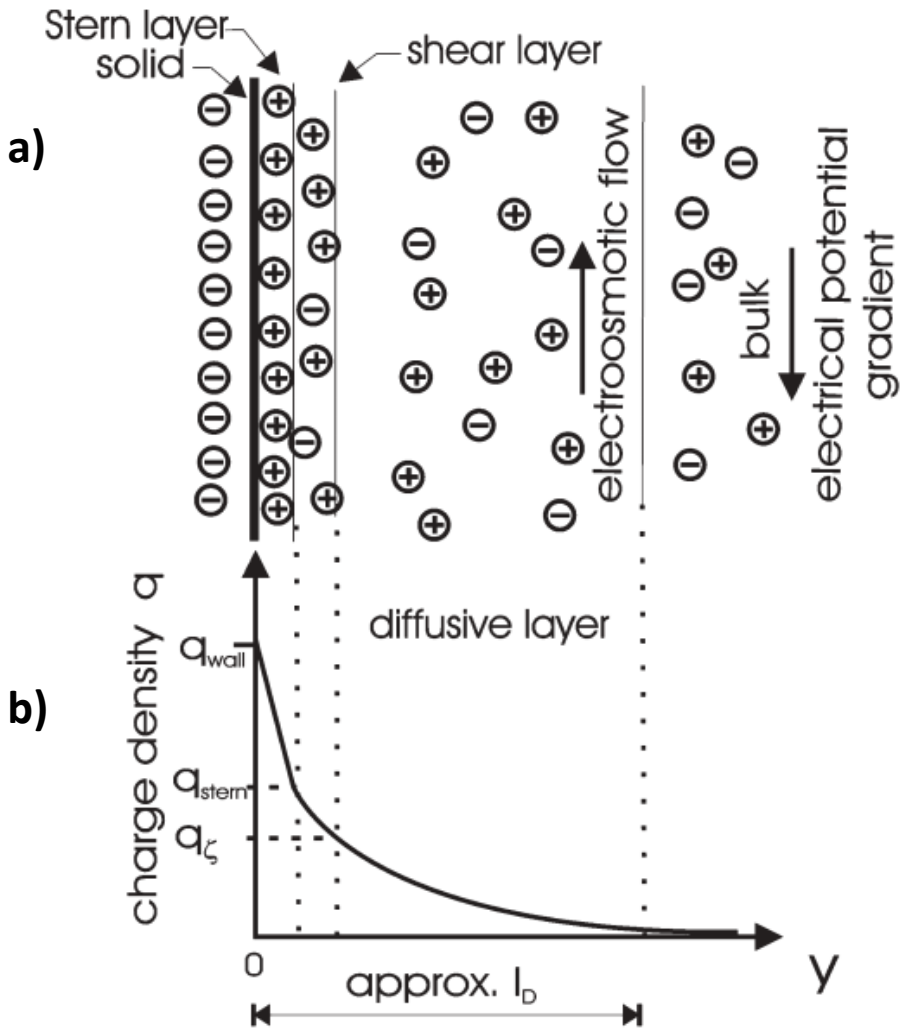

Figure 1.12. a) Schematic of electric double layer (EDL). The solid is represented by a vertical line of negative charges. Positive ions, represened by 'positive' circles are adsorbed to this surface, with the Stern layer boundary being denoted by a vertical line. Similarly, the shear layer is comprised of ions, and the boundry is denoted by a vertical line which is also considered the no-slip boundary (ζ). The diffusive layer is comprised of a less densly packed region of ions which screen the remaining charge. b) is a graphical representation of the charge density associated with the solution as a function of the distance from the charged particle [80]**. Reproduced by permission of The Royal Society of Chemistry.**

Surprisingly, as a result of this tendency of ions to screen out charged molecules in solution, the species of the ions used plays a role in how the molecule behaves in solution. In the case of DNA and solid-state nanopores, a number of monovalent ions have been used, and shown to have a large impact on translocation times [34], as highlighted in Figure 1.13.

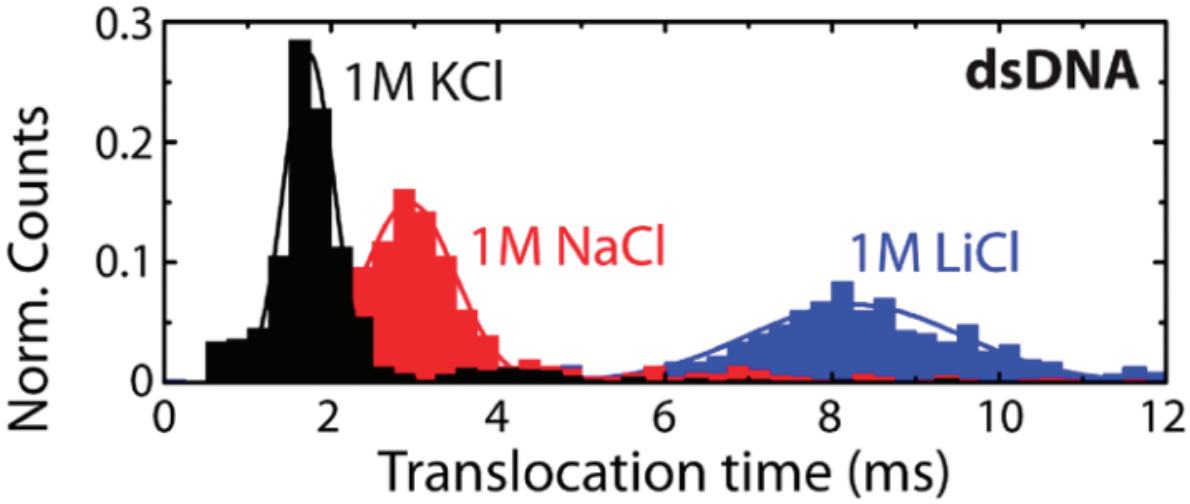

Figure 1.13. Histogram of 48.5 kbp DNA translocation events through 15-20 nm nanopores. Different elecotrlytes were used, as is demonstrated by the colour-coded histograms. Reprinted with permision from [34]. Copyright 2012 Americal Chemical Society.

This behaviour is attributed to the ability of smaller ions, such as Li^+, due to their ability to interact more strongly with the charged DNA molecule than larger monovalent ions, like Na^+ or K^+. As a result, the average time each ion is bound to the DNA molecule for different ions varies, with Li^+-DNA interactions surviving the longest, followed by Na^+, and finally K^+. Due to longer lasting interactions, Li^+ ions reduce the effective charge of DNA more than the other cations. As the translocation rate depends on the electrophoretic force on the DNA, this reduction in effective charge reduces the translocation speed of DNA. This dependency is presented in Equation 1.10 [81], which is tailored for DNA:

$$f(V) = z * e * \frac{n}{L} * V \qquad [1.10]$$

where $z * e$ is the effective charge of DNA inside the nanopore, V is the voltage that is applied, n is the number of nucleotides within the pore and L is the length of the nanopore.

Like any molecule, DNA in solution will try to minimize its free energy. In order to do this, the molecule will tend to minimize interactions with the surrounding solution, and as a result the time-averaged shape of a DNA molecule in solution is spherical [82]. dsDNA, however, is not overly flexible, and as a result behaves similarly to a series of semi-flexible rods joined end-to-end [83]. The length of these flexible rods is ~100 nm, and this length is termed the Kuhn length (L_k). Therefore, for very short dsDNA molecules where $L_k > L_{DNA}$, the molecule can be thought of as rod-like [83]. For long dsDNA molecules in solution, where $L_k << L_{DNA,}$ the conformation of the DNA will be a random walk with step size L_k. This results in a coil whose radius is called the radius of gyration (R_g) [83].

Finally, an important characteristic of DNA is that solvent molecules are able to flow through the coil and past any base along the strand with equal ease [84]. As a result, the coefficient of electrophoretic friction (φ) scales linearly with the number of DNA monomers. Additionally, since each monomer contains the same charge (Q), it too scales linearly with the number of DNA monomers, and DNA is therefore a free-draining polymer where molecules move through free solution under an applied electric field at a rate that is independent of molecular length (note: this breaks down for very short DNA molecules, where $L_{DNA} < 200$nm[85]). This is described in equation [1.10] [86]:

$$\mu_{DNA} = \frac{v}{E} = \frac{Q}{\varphi} \qquad [1.10]$$

where μ_{DNA} is the electrophoretic mobility of DNA, v is the electrophoretic velocity, E is the electric field strength, Q is the net charge of the DNA molecule and φ is the electrophoretic

friction coefficient. Since DNA cannot be easily separated in free solution, gels are often employed to retard the longer fragments more readily than shorter ones.

1.10.2 DNA in a Gel

In order to understand how a DNA molecule is moving through a gel, the size of the gel pores must be known. One large problem associated with determining these gel pore sizes is that each method of measurement tends to give a different reading, due to the inherent sampling bias of each different method [83,87]. For instance, determining the gel pore size in 1% agarose using the mobility of latex spheres results in an estimation of the diameter of 150 nm [88], while the use of an atomic force microscope yields greater than 400 nm in diameter [89]. This large spread affects our ability to predict the gel pore size, and therefore hinders our ability to choose a gel with the desirable properties to perform certain tests. Nevertheless, in order to keep the design as simple as possible, I utilized readily available gels, namely agarose and polyacrylamide.

1.10.2.1 Agarose

As mentioned previously, agarose can be characterized in a number of different ways, and each way tends to lead to a different size estimate. In fact, even different groups measuring agarose gel pore size with the same method will still see a discrepancy between their size estimations [83]. It has been hypothesized that a number of reasons could account for this,

including the differences between each batch of agarose, inherent flaws in each method, and history of the gel [83]. This essentially means that when talking about agarose gel, pore size measurements are a rough estimation. For the purpose of this thesis, I relied on an approximation that falls between the extremes, considering the diameter of the gel pores (d_{gel}) to be 300 ± 100 nm.

While the size of the agarose gel pores is relatively unknown, the important quality is that $d_{gel} > L_p$. Should we introduce a small DNA molecule into this agarose such that $R_g < d_{gel}$, the molecule would be able fold into a coil inside a single gel pore. If this coil of DNA exists in the agarose without any external forces (e.g., electric field) acting on it, it would remain within the gel pore until Brownian motion provided an escape. Conversely, if the DNA in question is large, such that $R_g > d_{gel}$, the DNA is be forced to reside in >1 gel pore in order to accommodate its size [83].

Agarose itself is a relatively rigid polysaccharide polymer, generally extracted from seaweed. It has low solubility in water at room temperature, but at high temperature it dissolves well and forms a physical gel upon cooling. Further information about the gelling system of agarose can be found at [90].

1.10.2.2 Polyacrylamide

Polyacrylamide, usually used for proteins or small DNA molecules, contains much smaller gel pores. Similar to agarose, polyacrylamide pore size is the subject of debate, and varies depending on the method used to measure the pores. Pore size has been estimated to range

from 5-100 nm, although the theoretical and electron microscope seem to agree fairly well that the mean pore size is centered around 10 nm [83].

Polyacrylamide is more flexible than agarose, although it undergoes proper crosslinking (more information available at [91]) unlike agarose, which causes a more rigid gel to form. The polyacrylamide solution contains both monomers of acrylamide and the cross-linker, bis-acrylamide. TEMED is used to induce free-radical generation from ammonium persulfate (APS), which in turn radicalize the acrylamide and bis-a, which then react with each other, forming a 3D network of chemically linked acrylamide polymers.

1.11 Choice of Gels

Different gels are able to provide different environments, making the choice of gel for an experiment critically important. In order for the gel on the *trans* side of the membrane to impact translocation dynamics, the DNA molecule must reside within the nanopore while simultaneously interacting with the gel. This condition focuses my research on the reptation regime, where $R_g > d_{pore}$ [83], because if this condition is not met, the DNA will have left the nanopore before encountering a gel fiber. It is important to mention that there are several field-dependent sub-regimes that exist within the reptation regime. However, due to the unconventionally steep decay of the electric field near the mouth of the nanopore, we argue it would be nearly impossible to deconvolute them, and thus they can only be considered globally. Therefore I focus on the reptation regime under two conditions: i) when the DNA molecule is flexible on the length scale of a gel pore ($d_{gel} > L_p$ where L_p = 50 nm for dsDNA)

and the polymer chain can easily deform when it is forced to invade the gel on the *trans* side; and ii) when the DNA behaves as persistent (rod-like) segments in tight gel pores ($L_p > d_{gel}$) [83], and pushing the chain through the gel does not lead to conformational deformations on the short length scales relevant to these experiments. These two regimes are achieved through the use of agarose and polyacrylamide gels, respectively. My experimental study will thus be able to explore these two very different limits.

Importantly, the movement of DNA through these gels is complex, and is related to no fewer than four length scales: L_p and R_g of the polymer, the mean gel pore size d_{gel}, and the convection length, R_c, defined as the distance from the nanopore beyond which Brownian motion dominates over the electrostatic forces (this length scale is analogous to the capture radius on the *cis*-side [36]). While the interplay between these four length scales may, in principle, predict the existence of numerous translocation regimes [83], only a few of them are relevant when realistic experimental values are considered, as shown below.

In order to estimate R_c, we can assume the electric field extends outwards from the nanopore in a radial fashion according to Ohm's law (assuming spherical symmetry) [92],

$$\vec{E}(r) = \frac{I_0 \vec{r}}{2\pi|r^3|\sigma} \qquad [1.12]$$

where I_0 is the baseline ionic current, σ is the conductivity of the solution, and r is the distance from the mouth of the nanopore. From Equation 1.12 we are able to determine that the electric field $\gtrsim 40\mathrm{V/m}$ extends several micrometers into the *trans* side, thus ensuring that any translocated molecules are ushered away from the nanopore, allowing for the next molecule

to translocate. This was typically found to be true, however as mentioned in 3.1, this wasn't always the case.

The following chapter is a published paper:

Waugh, M., Carlsen, A., Sean, D., Slater, G., Briggs, K., Kwok, H., and Tabard-Cossa, V. 2015. *Interfacing Solid-State Nanopores with Gel Media to Slow DNA Translocations*. Electrophoresis. DOI: 10.1002/elps.201400488

2 Interfacing Solid-State Nanopores with Gel Media to Slow DNA Translocations

Matthew Waugh, Autumn Carlsen, David Sean, Gary W. Slater, Kyle Briggs, Harold Kwok and Vincent Tabard-Cossa*

Department of Physics, University of Ottawa, Ottawa, Ontario, Canada

*To whom all correspondence (including galley proofs) is to be sent:

Vincent Tabard-Cossa, Ph.D.

Assistant Professor

Department of Physics

University of Ottawa

150 Louis-Pasteur, Rm MCD338J

Ottawa ON, K1N 6N5, Canada

Fax: (613) 562-5190

Email: tcossa at uOttawa.ca

Abstract

We demonstrate the ability to slow DNA translocations through solid-state nanopores by interfacing the *trans* side of the membrane with gel media. In this work, we focus on two reptation regimes: when the DNA molecule is flexible on the length scale of a gel pore, and when the DNA behaves as persistent segments in tight gel pores. The first regime is investigated using agarose gels, which produces a very wide distribution of translocation times for 5 kbp dsDNA fragments, spanning over three orders of magnitude. The second regime is attained with polyacrylamide gels, which can maintain a tight spread and produce a shift in the distribution of the translocation times by an order of magnitude for 100 bp dsDNA fragments, if inter-molecular crowding on the *trans* side is avoided. While previous approaches have proven successful at slowing DNA passage, they have generally been detrimental to the signal-to-noise ratio, capture rate or experimental simplicity. These results establish that by controlling the regime of DNA movement exiting a nanopore interfaced with a gel medium, it is possible to address the issue of rapid biomolecule translocations through nanopores – presently one of the largest hurdles facing nanopore-based analysis – without affecting the signal quality or capture efficiency.

2.1 Introduction

During a typical nanopore experiment, an applied voltage drives a stream of ions through a narrow pore in a thin membrane separating two fluidic reservoirs. The passage of a biomolecule through the nanopore displaces a corresponding volume of ionic solution, resulting in a measurable current change. Ideally, this method would be capable of differentiating between individual bases on a DNA molecule using the current signature collected from the unique blockage volume of each base [21,22,24]. However, due to the rapid translocation rate of DNA through biological and sub-10-nm solid-state nanopores (roughly 1 nt/μs and >10 bp/μs, respectively [33,93]), it is extremely difficult to collect a sufficient number of ions for each base to overcome background noise and signals from adjacent bases [22,25]. Thus, a critical step toward nanopore-based nucleic acid analysis is extending the time that DNA lingers in the nanoscale confinement of a nanopore (while minimizing the likelihood of backtracking due to Brownian motion), thereby enabling detection of more ions per sub-nanometer section of the strand. The slowing down of DNA translocation kinetics will not only allow sufficient signal averaging to resolve current differences required to sequence DNA [40,46] but may also benefit various diagnostic applications by allowing better identification of labels for multiplexed biomarker detection [94,95].

In pursuit of extending nanopore dwell times, researchers have modified three basic components of the nanopore system – the environment, the molecule of interest, and the nanopore itself. In terms of the environment surrounding the nanopore, both biological and solid-state nanopore researchers have experimented with reducing solvent temperature [29,30] and increasing viscosity [31–33]. Solid-state researchers have further explored the use of

alternate salts [14,34] and the introduction of a salt concentration gradient [35,36] or counter pressure [37,38], achieving close to 10-fold translocation rate reductions by these means [38]. However, since altering the nanopore environment influences the molecule of interest and the ions in solution equally, the gains in dwell time have generally come at the expense of other desirable attributes, such as high signal-to-noise ratio or capture rate.

Efforts to slow translocation have also focused on modifying attributes of the molecules of interest, employing molecular motors or tethering them to mechanical probes. For biological nanopores, the addition of bulky tags to the analyte was found to diminish translocation speed [39] while enzymes [25] permitted ratcheting (also called processive translocation [40–43]) and a closer look at DNA-enzyme interactions [44]. In fact, combining enzymes with an MspA nanopore [45] enabled single-nucleotide resolution [46] of ssDNA strands. Combining DNA hairpins [47–50] or avidin-bound ssDNA [51–53] with biological nanopores has facilitated slower translocation and repeated interrogation of the same molecule by physically blocking the molecule from completing its passage through the nanopore. Similar results have been achieved through the incorporation of optical tweezers [54,55], magnetic tweezers [56], or AFM tips [57] in solid-state nanopore experiments. While these modifications to the analyte have substantially slowed translocation rates to greater than tens of μs per base, it should be noted that a significant selling point for a nanopore-based system is high-throughput and scalability to obtain rapid results at low cost. Many of these approaches inherently add layers of complexity, while the ideal nanopore device would not require such modifications [21].

A final route to slowing translocations has involved modification of the nanopore itself. For example, modifications to solid-state nanopores have included adjusting the nanopore diameter to increase friction [58–60], modulating the nanopore surface charge with laser light

[61], functionalizing the nanopore with hydrogen-bonding molecules [62] or coating it with a lipid bilayer [63], and altering the properties of a pH-responsive organic film [64]. Additional methods have been proposed, including local heating of a gold layer surrounding the nanopore to stretch the DNA [65,66] and ratcheting of nucleotide strands through introduction of a third electrode [67,68]. In fact, researchers have investigated a three-terminal system, or field effect nanofluidic transistor, which would alter the electric field profile in the nanopore [69–71] and modulate its surface charge [72–75]. Base-by-base ratcheting using electrostatic traps in a DNA transistor has yet to be achieved, but nanopore modifications have already reduced translocation speeds by up to an order of magnitude for ssDNA [62,73].

Recently, the use of an alternative method for slowing translocations has been reported – a copolymer mesh electrospun on the *cis* side of a solid-state nanopore [76]. An approaching DNA fragment must first pass through the mesh then electrophoretically thread through the nanopore before exiting on the *trans* side. Although a promising approach – translocation rates were reduced by up to two orders of magnitude, reaching ~2 bp/μs – the copolymer mesh employed has not yet been fully characterized and requires extensive experimental preparation time. Our work is distinct from this in two ways: 1) we employ readily available, well-characterized materials – agarose or polyacrylamide – and 2) we deposit the film on the *trans* side of the nanopore, thus keeping the DNA capture process intact. The application of the gel medium exclusively on the *trans* side of a solid-state nanopore (Figure 2.1) with the objective of slowing DNA translocation kinetics also distinguishes our work from a previous publication that described deposition of agarose on either side of a biological nanopore to improve bilayer stability [96]. Our approach represents an important step toward cost-effective, rapid and simple nanopore-based diagnostic capabilities. We are able to slow the

translocation process while maintaining a high electric field strength, which is important for preserving a sufficiently high capture rate (or capture radius), ensuring detection of a larger number of ions flowing through the nanopore for a stronger signal, as well as overcoming the issue of DNA molecules backtracking within the nanopore due to Brownian motion.

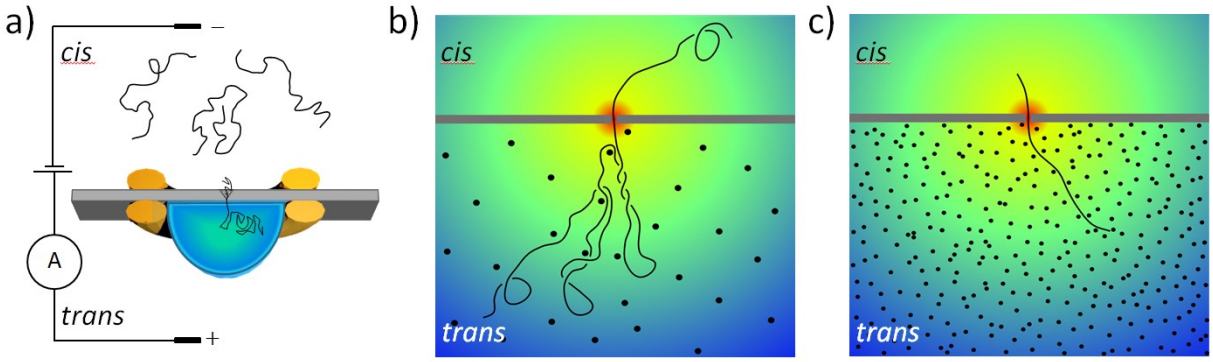

Figure 2.14. Schematic of the experimental system (not to scale). a) Elastomer gaskets contain a droplet of the gel solution (agarose or polyacrylamide) deposited on the *trans* side of a standard 10-nm thick SiN_x membrane (50-µm × 50-µm) on a Si chip. Following gelation of the polymer solution and subsequent mounting of the Si chip in a fluidic cell, a nanopore is formed through the SiN_x membrane by controlled breakdown (CBD). DNA is introduced to the *cis* side of the membrane and electrophoretically driven through the nanopore into the gel medium on the *trans* side. Schematic cross-sectional view of a DNA molecule entering into a gel medium from a nanopore, where b) satisfies the condition $R_g > d_{gel} > L_p$, similar to the case for agarose, while c) demonstrates the $R_g > L_p > d_{gel}$ limit, similar to the polyacrylamide system. In both schematics the electric field strength is illustrated by colour gradient, with red being greatest electric field strength, and blue the smallest.

In theory, no fewer than four length scales are needed to describe the movement of a charged polymer on the *trans* side of a nanopore membrane interfaced with a gel medium: the persistence length (L_p) and radius of gyration (R_g) of the polymer, the mean gel pore size (d_{gel}),

and the convection length (R_c), defined as the distance from the nanopore beyond which Brownian motion dominates over the electrostatic forces (this length scale is analogous to the capture radius on the *cis* side [36]). While the interplay between these four length scales may, in principle, predict the existence of numerous translocation regimes, only a few of them are relevant when realistic experimental values are considered, as described below.

In order to estimate R_c, we can assume the electric field extends outwards from the nanopore in a radial fashion according to Ohm's law (assuming spherical symmetry) [92],

$$\vec{E}(r) = \frac{I_0 \vec{r}}{2\pi|r^3|\sigma} \qquad [2.1]$$

where I_0 is the baseline ionic current, σ is the conductivity of the solution, and r is the distance from the mouth of the nanopore. From Equation 2.1, we are able to determine that the electric field extends several micrometers into the *trans* side, and will therefore push translocated DNA away from the nanopore and further into the gel, making room for other molecules.

In order to determine the most effective gel pore size for the *trans* side of the membrane, we consider the behaviour of DNA undergoing gel electrophoresis when the mean diameter of the gel pores, d_{gel}, is larger than, equal to, or smaller than the radius of gyration, R_g, of DNA. Firstly, $R_g < d_{gel}$ produces Ogston sieving. In this regime, the DNA molecule must travel a distance larger than R_g before encountering a gel fiber, meaning that in our system it could not interact with a gel fiber and be within the nanopore sensing region simultaneously. Therefore Ogston sieving mechanisms cannot easily be exploited to slow down DNA translocation through the nanopore. Similarly, the short entropic trapping regime that replaces Ogston sieving when $R_g \approx d_{gel}$ does not offer many DNA-gel fiber interactions while the DNA

molecule resides within the nanopore, and would not be conducive to slowing DNA translocation. For this reason, we focus on the reptation regime where $d_{gel} < R_g$ [83]. It is important to mention that there are several field-dependent sub-regimes that exist within the reptation regime. However, due to the unconventionally steep decay of the electric field near the mouth of the nanopore, we argue it would be nearly impossible to deconvolute them over the R_c length scale, and thus they can only be considered globally. Therefore we focus on the reptation regime under two conditions: i) when the DNA molecule is flexible on the length scale of a gel pore ($d_{gel} > L_p$ where L_p = 50 nm for dsDNA) and the polymer chain can easily deform when forced to invade the gel on the *trans* side; and ii) when the DNA behaves as persistent (rod-like) segments in tight gel pores ($L_p > d_{gel}$) [83], and pushing the chain through the gel does not lead to conformational deformations. These two regimes are achieved through the use of agarose and polyacrylamide gels, respectively. Our experimental study will thus be able to explore these two different limits.

2.2 Materials and Methods

2.2.1 Silicon Nitride Membranes

The silicon nitride (SiN_x) membranes utilized for our experiments were acquired from Norcada (Edmonton, Alberta), and are commercially available as transmission electron microscope (TEM) windows. The membranes are composed of 10-nm thick low-stress SiN_x deposited on a 200-µm thick Si substrate by low pressure chemical vapour deposition (LPCVD). An anisotropic wet chemical etch is then used to produce a 50-µm x 50-µm

freestanding membrane in the center of a 3-mm silicon support chip. Before depositing the gels on the membranes, the chips were cleaned in oxygen plasma for 1 minute at 50 W.

2.2.2 Polymer Gels

2.2.2.1 Agarose

1% (w/v) UltraPure agarose (Invitrogen, Carlsbad, CA) was dissolved in a heated 10 mM KCl solution (pH 8). The solution temperature was maintained at 60°C for ~45 minutes to ensure equilibrium had been reached. Any water that had evaporated was replaced with degassed DI water and the solution was briefly degassed again. A droplet (~2 µL) of the agarose solution was then pipetted onto the SiN_x membrane, with a silicon elastomer gasket offering containment and support to the liquid as it gelled. The resulting agarose gel thickness was estimated at ~1.5 mm. Note that the applied voltage was largely unaffected by the presence of the gel, as the resistance across it was measured to be <1% of that of the agarose-interfaced nanopore system.

2.2.2.2 Polyacrylamide

Ultra-Pure Acrylamide, Bis and N,N,N',N'-Tetramethylethylenediamine (TEMED) were purchased from Fisher (Pittsburgh, PA). The concentration of acrylamide was 10%, and a Bis concentration of 0.8% was used. The gel also contained 380 mM Tris (pH 8.8), 10 mM KCl, 0.1% ammonium persulfate and 0.1% TEMED. A droplet (~2 µl) was placed on the membrane, in the same manner as with the agarose. The gel was left for at least 3 hours for

polymerization to occur. Each gel was visually inspected and confirmed to be solid before chips were mounted in the fluidic cells. The measured resistance across the polyacrylamide gel constituted ~2% of the total resistance of the polyacrylamide-interfaced nanopore system.

2.2.3 Fluidic Cell and Mounting Procedure

Once the gel solution had been placed on one side of the chip and allowed to solidify, the device was mounted in a polyether ether ketone (PEEK) fluidic cell, with custom-made silicon elastomer gaskets, ensuring a liquid-tight seal. The reservoir on either side of the chip was filled with ~250 µL of a 1M KCl solution (pH 8), buffered with 10mM HEPES. A pair of Ag/AgCl electrodes was used to apply the potential and measure the current, with the electrode on the *trans* side being grounded. All voltages are applied to the *cis* electrode with respect to ground. While a custom electronic circuit was employed during the nanopore fabrication process [16], an Axopatch 200B monitored the ionic current and supplied the voltage during the DNA experiments.

2.2.4 DNA Experiments

50 bp, 100 bp, and 5 kbp dsDNA were purchased from Fermentas (Thermo Scientific, Pittsburgh, PA). The concentration of DNA employed for the experiments was ~6 ng/µL. Occasionally, the nanopores would become clogged and were cleared by reversing the voltage polarity. Custom LabView programs were used for data acquisition and analysis, and a National Instruments (Austin, TX) DAQ card (NI PXIe-6363) was used for data acquisition.

The ionic current signal was acquired at 250 kHz and low-pass filtered at 100 kHz with a four-pole Bessel filter.

2.3 Results and Discussion

We previously reported the fabrication of solid-state nanopores by controlled breakdown (CBD) of a thin dielectric membrane in an aqueous electrolyte environment, where an applied voltage produces an electric field strength >0.5 V/nm and generates a sustained leakage current through an otherwise insulating membrane [16,60]. In order to investigate the effects of a nanopore interfaced with a gel on DNA translocation kinetics, we deposit the gel medium on an intact SiN_x membrane, mount the gel-interfaced membrane in a fluidic cell and then fabricate a nanopore by CBD. We expect the dielectric breakdown process to be more likely to occur in a relatively fiber-free area at the gel/membrane interface, due to the greater availability of ions for charge injection[97] . In this case, a DNA strand exiting the nanopore will initially enter a solution-filled void before encountering gel fibers. The molecule will then begin the process of finding a route through the gel. Analysis of the results obtained from DNA translocation experiments are reported below.

2.3.1 Nanopore Fabrication by CBD

Nanopore fabrication is carried out in 1 M KCl or 3.6M LiCl (pH 8) with a constant applied voltage ranging from -7 V to -9 V. During fabrication, a leakage current on the order of tens of nA is monitored. The charge transport mechanism through the dielectric membrane

involves a form of trap-assisted electron tunnelling [16] which results from charge injection at the electrolyte/membrane interface by specific redox reactions [97], the nature of which depends on the type of ions present within the electrostatic double layer surrounding the membrane. The fabrication of nanopores in SiN_x membranes interfaced with a gel reveals kinetics and a magnitude in leakage current similar to bare membranes under otherwise analogous conditions. Once the nanopore is successfully fabricated, its conductance is extracted from the slope of the I-V curve, which allows for the estimation of the effective diameter of the nanopore [12,97].

Some nanopores formed in this manner display typical characteristics of bare CBD-fabricated nanopores, with well-defined breakdown events and nearly linear I-V curves. While these nanopores are stable and exhibit typical low-noise behaviour, others behave anomalously, either clogging or rectifying strongly. Predictably, these anomalous nanopores produce current traces that are much noisier than those of ohmic nanopores. Another potential source of anomalous behavior – the delamination of the gel interface from the nanopore – was observed only once, resulting in no polyacrylamide-induced change in the translocation kinetics for 5kbp dsDNA. Overall, the yield for formation of low-noise nanopores successfully interfaced with agarose or polyacrylamide gel was ~31% (N = 16) and ~42% (N = 12), respectively. Out of the low-noise gel-interfaced nanopores, ~60% (N = 10) produced a few hundred translocations at various voltages or over a thousand at a single voltage before irreversibly clogging. Since the CBD fabrication method produces nanopores capable of DNA detection with a yield of ~80% on bare membranes [16], we attribute this relatively low yield (~21%) to the presence of the gel.

2.3.2 Nanopores Interfaced with Agarose Gel

We first consider the regime $R_g > d_{gel} > L_p$. Here, a full-length DNA molecule must occupy several gel pores, with each gel pore being large enough to accommodate multiple flexible segments of DNA, as depicted in Figure 2.1b. In order to satisfy these conditions, we use 1% agarose in 10 mM KCl, which results in an estimated d_{gel} of ~200-400 nm [98,99], interfaced with a nanopore 3.6 nm in effective diameter, to which we introduce 5 kbp dsDNA (R_g ~470 nm and contour length of 1.7 μm). Note that this nanopore size is chosen to ensure single-file passage of dsDNA, while at the same time avoiding translocations in the friction-dominated regime [58,60]. As shown in Figure 2.2, agarose slows down some of the DNA molecules substantially, by as much as 3 orders of magnitude (from tens of μs to tens of ms), while other DNA molecules pass through the gel with a dwell time similar to that observed in a bare nanopore of similar dimensions. The mean translocation time of the data plotted in Figure 2.2a is calculated to be 35 ±0.9 μs for the bare nanopore, while the agarose-interfaced nanopore has a mean translocation time nearly two orders of magnitude greater, at 2,900 ±470 μs. The wide distribution in the agarose-interfaced case is highlighted by the percentage of events longer than twice the mean; while roughly 3.5% of bare-nanopore events are longer than 70 μs, 15% of the agarose-interfaced nanopore events are longer than 5,700 μs.

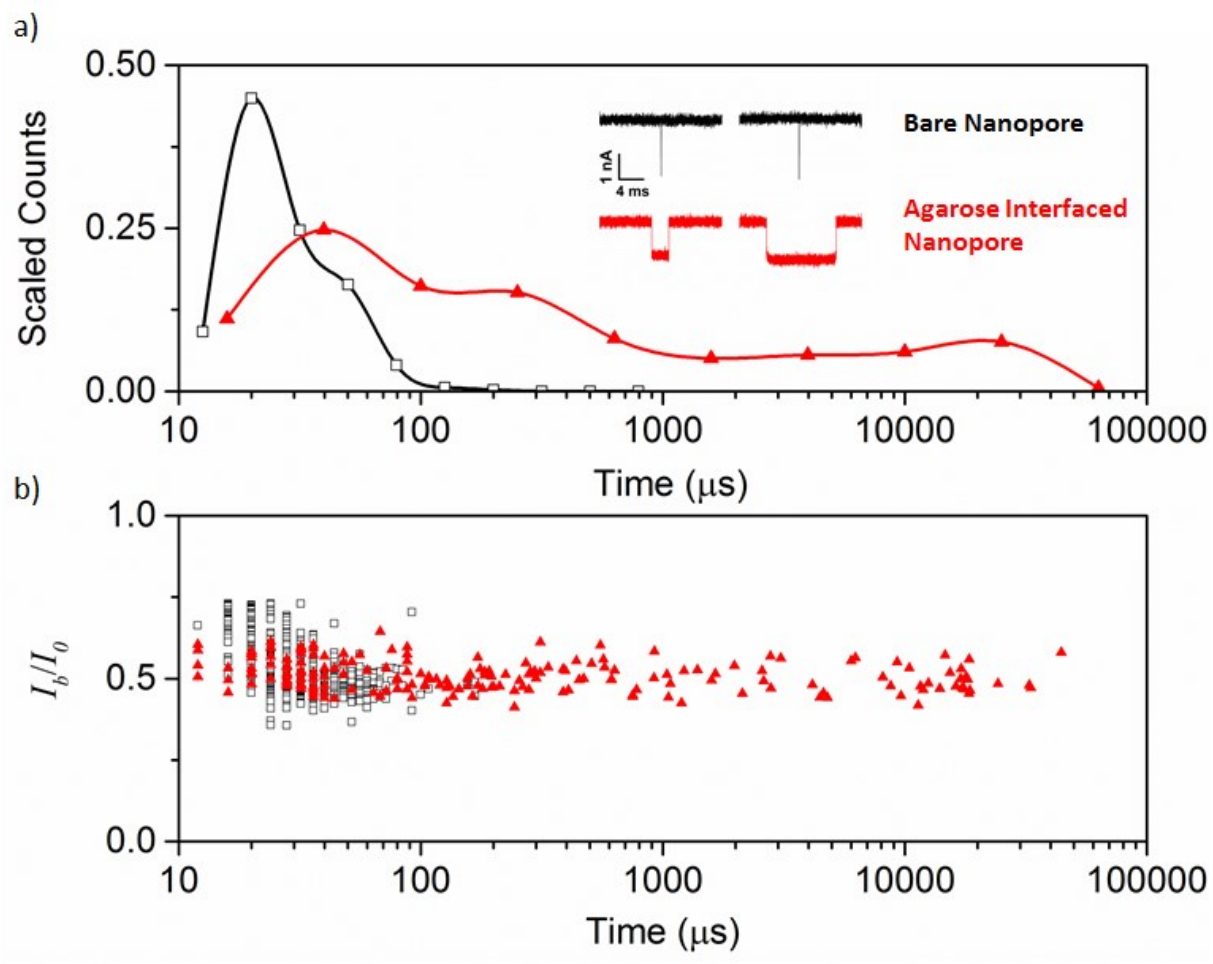

Figure 2.2. Comparison of 5 kbp dsDNA translocations through two similarly sized nanopores, one bare (4.1 nm) and the other with a *trans*-side agarose interface (3.6 nm). (a) Translocation time histograms reveal extended event durations for the agarose-interfaced nanopore versus the bare nanopore. Inset shows typical events for both cases. The events are 20 μs and 24 μs (left and right, respectively) for the bare nanopore, and 2,800 μs and 10,440 μs for the agarose-interfaced nanopore (left and right, respectively). (b) Scatterplot of the current blockade versus translocation time shows similar blockage levels for the agarose-interfaced and bare nanopores. Each data point represents an individual DNA translocation event (N_{bare} = 467; N_{gel} = 206). All measurements were performed in 1M KCl (pH 8) at -600 mV. Folded DNA translocations and partial translocations (collisions) were excluded for simplicity. Signals from molecules translocating more rapidly than ~20 μs will be increasingly truncated due to bandwidth limitations of the Axopatch 200B. This is also observed in b) and in Figure 2.3 and Figure 2.4, where the shallower blockages plotted for molecules translocating faster than ~20 μs are due to erroneous readings of the blockage depth (I_b). This does not affect our conclusions.

We attribute the overall increase in mean passage time to the DNA molecule interacting strongly with the gel on the *trans* side of the nanopore. There are two possible mechanisms for this interaction – electrical and steric. In terms of electrical (or charge-based) interactions, we might expect anion-binding centers in the agarose fibers [87] to interact with the highly negatively charged DNA molecules. However, the small number of sulfate groups (<0.15%)

combined with the screening effects of the high salt concentration in our agarose gel [100] ensure that this interaction will be minimal [101]. Instead, the principal mechanism for DNA-gel interactions should be steric in nature. During translocation through a bare nanopore, the leading end of a DNA molecule moves away from the nanopore while the rest of the molecule progresses through. The translocation kinetics in this case are usually dominated by the viscous drag of the portion of the molecule being pulled through the nanopore or by DNA-pore wall interactions [38,102]. However, when the nanopore is interfaced with a gel, the biomolecule may be sterically hindered during passage, essentially resulting in the molecule crowding itself, where the portion of the DNA molecule that has not yet translocated through the nanopore cannot translocate until the fraction of the molecule on the *trans* side vacates the gel pore in the immediate vicinity of the nanopore.

While the shift in mean passage time is remarkable, the wide spread in the distribution suggests that some molecules are interacting with the gel differently than others, which can be undesirable for some applications and increases the complexity of data analysis. We attribute this result to the stochastic behaviour of DNA in agarose gels when subjected to high electric fields, specifically the propensity of DNA to undergo geometration (hooking) and herniation of loops (branching) around the agarose fibers [83]. These retardation mechanisms are randomly triggered by thermal fluctuations and/or sampling of various gel fibre configurations. Although numerous models can be used to predict DNA electrophoretic mobility within gels, they actually describe the mean effect of a large number of retardation events taking place over a considerable migration distance. In the context of slowing down the DNA translocation process in nanopores, however, each molecule can only be affected by a small number of retardation events, leaving little room to account for all of the different

paths the DNA can take, which likely contributes to the spread of the distribution. In other words, differing translocation events arise from the various possible pathways through the gel. The large spread in translocation times should not be surprising, given that geometration and herniation, frequent under these conditions in the gel, introduce large variability in the DNA migration process [103–105]. For the same reasons, we do not anticipate all devices to behave identically. While we can easily fabricate a nanopore with controlled dimensions at the interface of the gel, we are unable to control the distribution of gel fibers near the nanopore. Therefore, while global trends pertaining to the increase in mean passage times and significant broadening of the distribution of translocation times are expected to persist, each device will show slightly different slowing characteristics as a result of variations in the gel (see Figure S1).

To test the gel's slowing effects on a smaller molecule (with $R_g < d_{gel}$), we perform translocations with a 50 bp dsDNA fragment (rod-like with length of ~17 nm) through a 6.0 nm nanopore interfaced with a 1% agarose gel. The resulting data agrees very well with a similar nanopore that was left bare (Figure 2.3). Not accounting for the potentially large fraction of events passing through both the bare and the agarose-interfaced nanopores too rapidly to be detected, the mean observable translocation times are similar, at ~10 μs. This is expected, as the 50 bp DNA only occupies a fraction of the void in the agarose, and therefore cannot both reside in the sensing region and interact with the gel fibers at the same time.

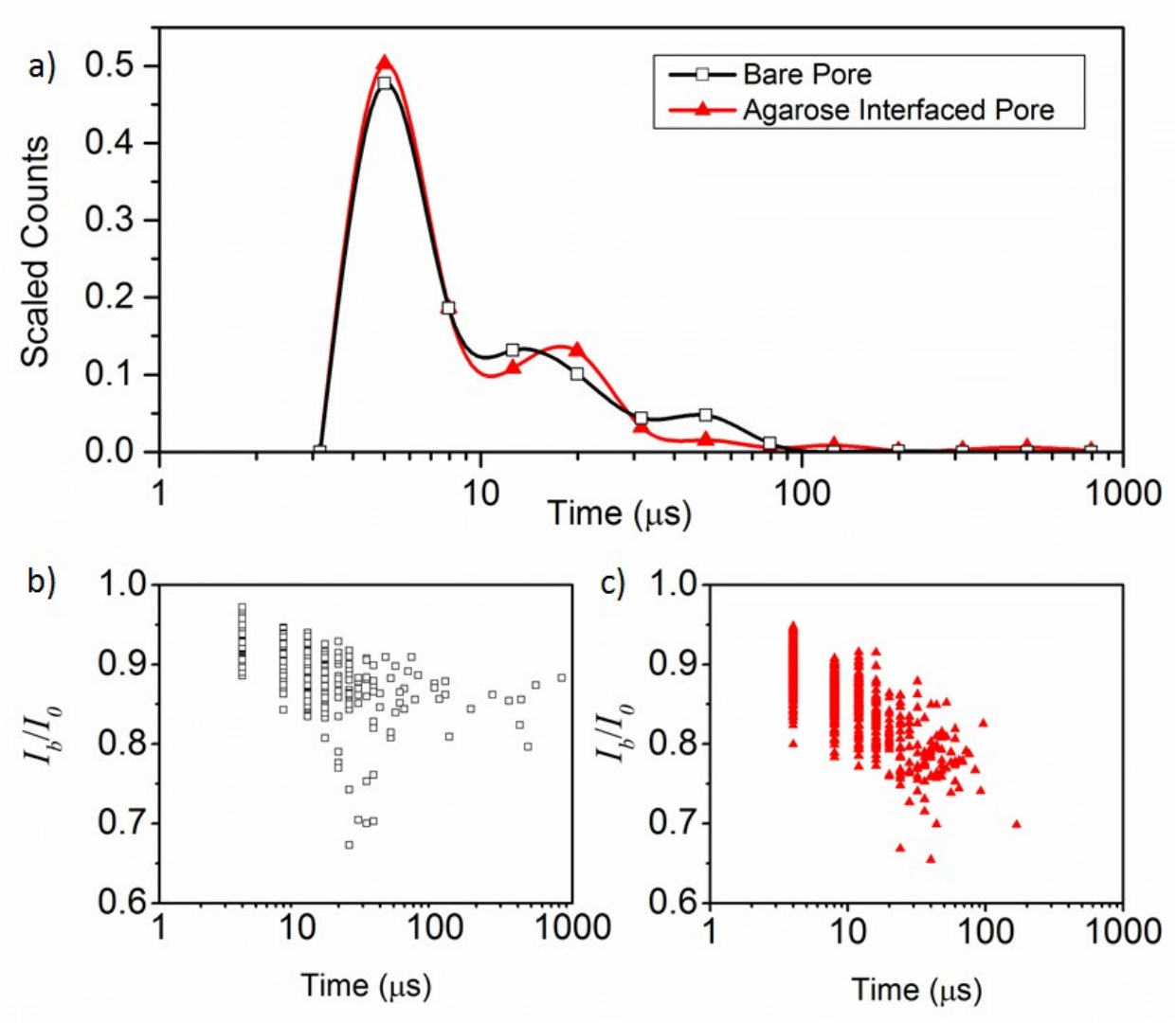

Figure 2.3. Comparison of 50 bp dsDNA translocations through two similarly sized nanopores, one bare (7.4 nm) and the other with a trans-side agarose interface (6.0 nm) (a) Translocation time histograms reveal nearly identical event durations for the agarose-interfaced nanopore versus the bare nanopore. Note that, due to limited bandwidth, it is very likely that many molecules are translocating undetected. The peak in the distribution should therefore not be regarded as the most probable passage time. (b) Scatterplot of the normalized current blockade versus translocation time shows very similar blockage levels for the agarose-interfaced and bare nanopores. Each data point represents an individual DNA translocation event (N_{bare} = 726; N_{gel} = 821). All measurements were performed in 3.6M LiCl (pH 8) at -200 mV. Events corresponding to folded DNA translocations were excluded for clarity.

2.3.3 Nanopores Interfaced with Polyacrylamide Gel

In response to the broad range of translocation times obtained with agarose-interfaced nanopores, we determined that much tighter gel pores are needed to provide more consistent steric hindrance during translocation events. Under these tight gel-pore conditions, herniation is unlikely to occur, so the molecule is forced to remain more or less linear, leading to fewer translocation conformations and reducing the spread of the translocation distribution. For this reason, we turn our attention towards the $L_p > d_{gel}$ regime (as shown in Figure 2.1c).

While entering this regime with agarose would be difficult, polyacrylamide, an equally well-characterized gel, is commonly employed in gel electrophoresis and possesses smaller gel pores (d_{gel} ~5-100 nm, with average gel pore size likely to be ~10 nm [83]). This should increase the likelihood of DNA-gel interactions while reducing the issue of herniation. Thus we expect that DNA will translocate into a more confined environment in polyacrylamide than it does in agarose, leading to more predictable translocation characteristics. This expectation is confirmed by the analysis of 100 bp DNA (rod-like with a length of ~34 nm) translocations through a nanopore interfaced with polyacrylamide. As shown in Figure 2.4, a 3.6-nm nanopore interfaced with a polyacrylamide gel strongly interacts with the rod-like DNA, essentially slowing each 100 bp molecule. The mean translocation time for the polyacrylamide-interfaced nanopore is measured to be 248 ±6 μs, nearly an order of magnitude slower than the 33 ±1 μs mean passage time through a similarly sized bare nanopore. This translates into ~0.4 bp/μs, a step towards achieving the necessary translocation speed for DNA sequence analysis. Importantly, the spread in translocation times is, in this case, spanning only ~170 μs (as calculated from the FWHM). The preservation of the

distribution spread is highlighted by the number of translocations at twice the mean; for the bare nanopore, ~4.8% of the events are slower than 66 μs, while for the polyacrylamide-interfaced nanopore, ~5.5% of the events are slower than 496 μs. However, as previously mentioned, the precise size of the gel pores in the vicinity of the nanopore is not easily controlled, and it is expected that the distribution of gel pore size encountered by the DNA as it moves out of the nanopore and through the gel, will influence the details of the translocation kinetics. In fact, Figure S2 reveals that not all polyacrylamide-interfaced nanopore devices will behave identically. While the most probable passage time is still shifted by over an order of magnitude, the histogram of translocation times contains a characteristic shoulder that widens the distribution considerably. Upon closer inspection, we find that the long duration translocation events occur exclusively when the molecule translocates immediately after the previous one (Figure S3). The observed correlation between translocation time and the time elapsed since the previous translocation is consistent with the idea that the translocating molecule can interact with other molecules within the *trans* side gel. This is not surprising, as the purpose of utilizing a *trans* side gel is to restrict the mobility of DNA during and after translocation.

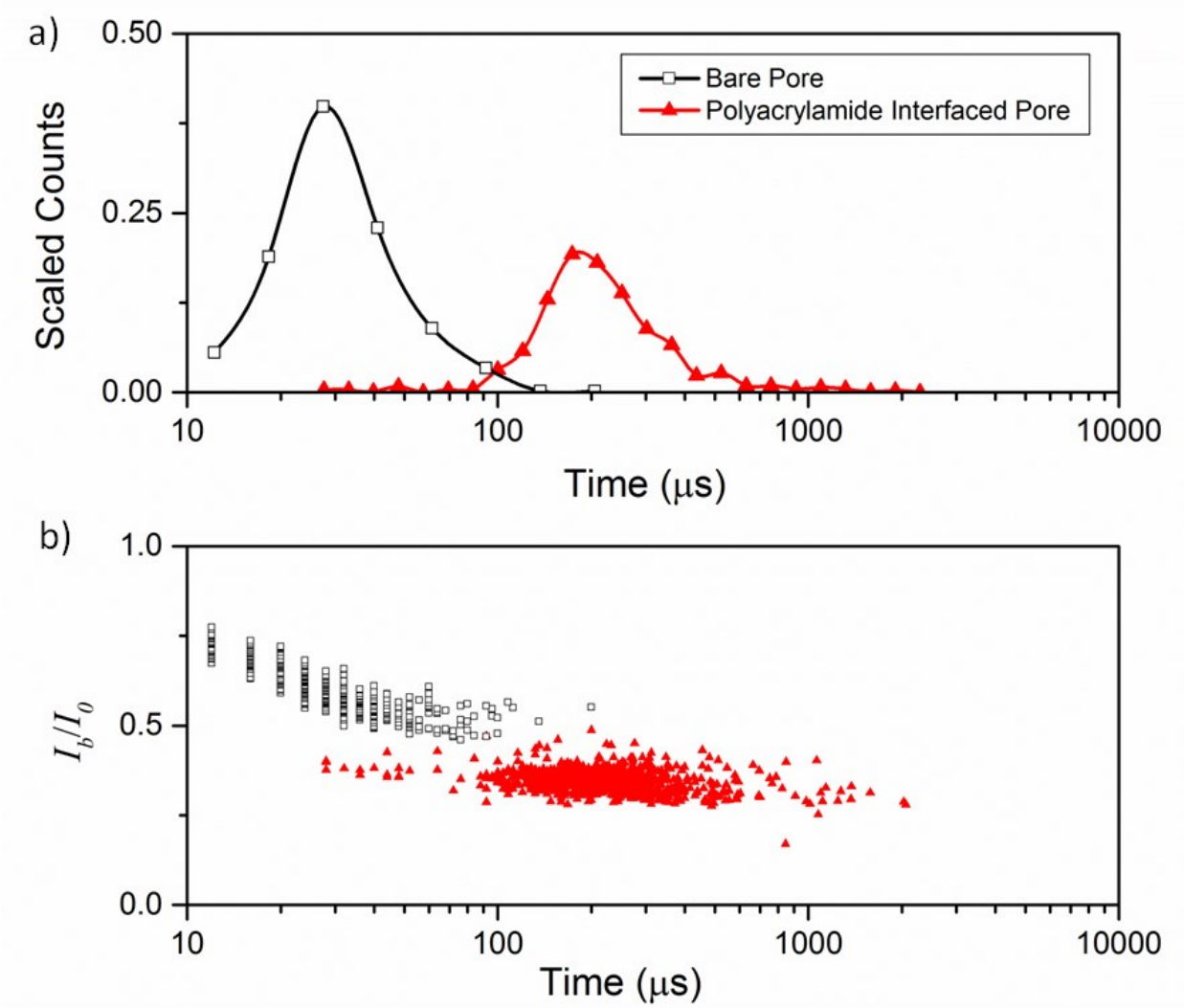

Figure 2.4. Comparison of 100 bp DNA translocations through two similarly sized nanopores, one bare (4.0 nm) and the other with a *trans*-side polyacrylamide interface (3.6 nm). (a) Translocation time histograms reveal extended event durations for the polyacrylamide-interfaced nanopore versus the bare nanopore. Note that, due to limited bandwidth, it is very likely that many molecules are translocating through the bare nanopore undetected. The peak in the distribution should therefore not be regarded as the most probable passage time for the case of the bare nanopore. (b) Scatterplot of the current blockade versus translocation time for both the polyacrylamide-interfaced and bare nanopores. Each data point represents an individual DNA translocation event (N_{bare} = 518; N_{gel} = 847). All measurements were performed in 3.6M LiCl (pH 8) at -400 mV. Partial DNA translocations (collisions with the nanopore) were observed but excluded for clarity.

The significant structural differences between agarose and polyacrylamide are further emphasized by efforts to translocate the much longer 5 kbp dsDNA molecules. As described

earlier, an agarose interface slowed the mean translocation time of 5 kbp fragments; however, the polyacrylamide interface slows the 5 kbp fragments to the extent that very few are even able to complete full translocation through the nanopore, and instead remain within the nanopore for several minutes until the voltage is altered to clear the nanopore.

2.4 Concluding Remarks

We showed that DNA translocations through a solid-state nanopore can be slowed down by interfacing the membrane on the *trans* side with a well-characterized and inexpensive gel medium – agarose or polyacrylamide – prior to fabricating a nanopore by CBD. A nanopore interfaced with agarose in this way produced a mean translocation time for 5kbp dsDNA nearly two orders of magnitude slower than a similarly sized bare nanopore operated under the same conditions. However, the distribution of event lengths observed with the agarose-interfaced nanopore spanned over three orders of magnitude. This large variance in the translocation times suggests that the agarose gel does not offer the continuous friction needed in order to slow down the molecules uniformly, and that there are simply too many routes for the DNA to take once inside the gel. Consequently, polyacrylamide-interfaced nanopores were used in order to exploit their tighter gel pores. These presented an order-of-magnitude shift in the mean DNA translocation time with nearly every individual 100 bp dsDNA molecule being slowed, permitting observation of the entire distribution of translocation times despite the short length of the fragments and the relatively high voltages used. We attribute the slowing efficiency of the polyacrylamide to a higher probability of interactions between DNA and polyacrylamide fibers, which presents a more stable network of tighter gel pores

compared to agarose. Additionally, inter-molecular crowding on the *trans* side, a rather unlikely interaction for typical translocation experiments, was found to contribute an additional retardation mechanism for some nanopores. However, when inter-DNA crowding was present on the *trans* side, it came with an additional broadening mechanism.

In summary, the use of a gel medium interfaced on the *trans* side of a solid-state nanopore significantly slows the translocation speed of DNA without affecting the capture process from the *cis* side. The use of commonly employed agarose and polyacrylamide as gel media ensures that this approach is both economical and accessible. In future work, the gel medium could be used to recapture previously translocated biomolecules by reversing the polarity of the voltage for repeated analysis, or pre-loaded with molecules as a means to rapid nanopore-based analysis on minute quantities of biological sample.

2.5 Acknowledgements

This work was supported by the Natural Sciences and Engineering Research Council of Canada (NSERC), and the Canada Foundation for Innovation. K. Briggs and M. Waugh acknowledge the financial support provided by NSERC, and OGS respectively, for Postgraduate Fellowships. The authors would like to thank Dr. James Harden for kindly granting the use of his polyacrylamide reagents.

The authors have declared no conflict of interest.

3. Conclusion

3.1 Summary

The speed with which DNA passes through solid-state nanopores continues to be one of the most pressing issues associated with the nanopore-based technology, and must be overcome if nanopores are to make a significant impact as a research or diagnostic tool. In this thesis I have demonstrated the ability to partially address this matter by interfacing the *trans* side of a solid-state membrane containing a solitary nanopore with a gel. While a number of other methods have been developed that are similarly geared towards slowing the passage of DNA molecules through solid-state nanopores, they are typically detrimental to the signal-to-noise ratio and/or the capture rate of the system. In contrast, by applying a gel to the *trans* side of the membrane, we do not affect the signal to noise ratio or capture rate in any appreciable way.

In order for the translocation rate of a molecule to be affected by a gel interfaced on the *trans* side of a solid-state membrane, it must interact with the gel while simultaneously residing within the sensing region of the nanopore. This occurs in what is termed the reptation regime of gel electrophoresis, where $d_{gel} < R_g$. When this is the case, the molecule should always encounter gel fibers before leaving the nanopore sensing region, and can thus be impacted during the passage through the nanopore. It is under these conditions that the experiments of this thesis were carried out. In order to fully understand the interaction between the DNA and the gel, I made use of two different gels (agarose and polyacrylamide) that shaped the *trans* side environments. This allowed for the investigation of two ends of the reptation regime spectrum, highlighting not only the ability of the gel to reduce the translocation speed of the

DNA molecules, but also the mechanism for how the gel was impacting and interacting with the molecules.

For the first environment, where $L_p < d_{gel} < R_g$, agarose-interfaced nanopores were used in conjunction with a long DNA fragment (5 kbp). Here, the gel pores were large enough to permit the polymer to fold on itself within a gel pore forming DNA blobs, while the DNA fragment was large enough such that it had to occupy multiple gel pores simultaneously. I believe this combination caused some molecules to herniate and hook around gel fibers as they exited the nanopore and entered the *trans* side of the membrane, which resulted in the leading end of the DNA molecule becoming momentarily stuck in the gel. The remaining portion of the molecule had to wait for the leading part of the strand to vacate the area near the nanopore before it could continue to translocate, thus increasing the translocation time. The result of these experiments was that I was able to drastically slow down some DNA molecules by over 3 orders of magnitude, while others remained unaffected. Because the retarding events were the result of a stochastic process, the distribution of dwell times was very wide.

Importantly, through the use of 50 bp DNA molecules and an agarose-interfaced nanopore, we were able to access the Ogsten sieving regime, where $d_{gel} > R_g$. Here, the DNA was too short to interact with the gel fibers while also residing within the sensing region of the nanopore. The experimental results confirmed what was expected, which was that the gel would have no impact on these short DNA fragments. This demonstrated that the agarose on the *trans* side of the nanopore was able to slow down molecules as long as the condition $d_{gel} < R_g$ was satisfied.

Using polyacrylamide as the interfacing gel, in contrast to agarose, formed gel pores on the order of 5-100 nm and satisfied the condition of $L_p > d_{gel}$, where the DNA cannot form a coil in the gel and must instead remain more rod-like near the nanopore. Due to the smaller size of the gel pores, the 5 kbp molecules had difficulty completing translocation through the nanopore as they would enter energy wells too deep to be overcome by the electric field on the timescales of the experiment. This led to the nanopore clogging, and would sometimes end the experiment. In order to circumvent the issue of molecular clogging within the nanopore, small DNA molecules (100 bp) were employed, as they would be unable to herniate or hook around the gel fibers due to the stiffness of the DNA backbone. With this experimental setup, the small molecules were able to translocate through the nanopore in a more reproducible way, which we attribute to the reduced number of conformations the molecule can take. Overall, the result was that the distribution of DNA translocations was shifted by roughly one order of magnitude while maintaining a relatively tight distribution. It was shown, however, that if a molecule encountered friction great enough that it could not vacate the region around the nanopore before the next molecule began to enter the gel, the second molecule would be forced to stay in the sensing region of the nanopore for longer. This is shown in Figure 3.1, which demonstrates that molecules that took longer than 1 ms to translocate did so mostly because they were preceded immediately by another molecule.

Unfortunately, this highlights one of the drawbacks of the *trans*-side gel-interface method: due to the stochasticity of the formation of gel pores, I am unable to control the gel pore size in the vicinity of the nanopore. The result of this is that two experiments performed under similar conditions will often yield slightly different results. While this is clearly undesirable,

the difference between two successive experiments is minor, as long as intermolecular crowding is avoided.

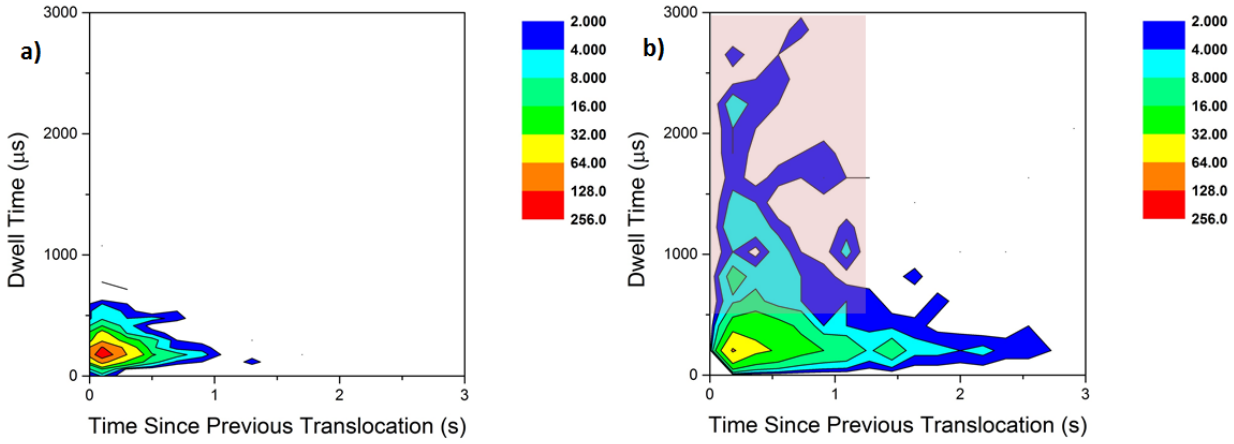

Figure 3.1. Relationship between inter-event time and translocation event length for two nanopores interfaced with poly acrylamide gel operated at 200 mV. The DNA molecules used in this experiment were 100 bp in length. In a), the 3.6-nm nanopore (Figure 2.4) shows a tight distribution of dwell times. In b), the 6.4-nm nanopore shows a strong correlation between time since previous translocation and dwell time. The pink highlighted rectangle in b) emphasizes the fact that nearly all the translocations lasting longer than 500 µs occur when the molecule translocates within a relatively short timeframe after the previous translocation. This lends itself to the idea that the previous molecule crowds the next one, leading to longer translocation events, and a smearing in the translocation times. Conversely, a) suggests the time since the previous translocation has little impact on the dwell time for the nanopore presented in the main text, maintaining a tight distribution seen in Figure S2a (red triangles).

3.2 Outlook

The success of the *trans*-side gel-interfaced solid-state nanopore opens the door to many potential avenues of research. One of the key experiments of future work is to tune the pore size of the appropriate gel so the gel pores are conducive to a regime where the gel limits the number of conformations of the translocating DNA, while simultaneously allowing for the

passage of long DNA molecules without clogging the nanopore. This would likely be time consuming, but could lead to a significant reduction in DNA translocation speed and allow for the interrogation of long DNA molecules.

Unfortunately, even if the gel pore size is tuned, one of the largest questions will be surrounding how the DNA molecule is moving. Ideally, the molecule will be slowed uniformly such that every point of the molecule travels at the same rate, providing simplicity for analysis. This research may prove very difficult, as any velocity measurement [106] will have to make use of a size marker on the DNA molecule, likely in the form of a radial protrusion or a nick in the DNA, both of which would alter the movement of a DNA molecule through the tight confines of a gel. Instead, it is possible that simulations would be able to determine the velocity profile of a translocating molecule.

One key feature of using gel at the membrane interface is that the gel can be loaded with some molecule or sample. Presently, a DNA sample that is of interest is injected into the bulk solution, which can be on the order of several hundred microliters. For a precious sample this may be too dilute to obtain a capture rate that is conducive to analysis. By forming the gel with the molecule of interest pre-loaded into it, the molecule will already be near the nanopore at a high concentration, facilitating the observation of minute samples.

Finally, and perhaps the most relevant for sequencing technologies, is the use of gel-interfaced nanopores passing ssDNA. In order to obtain information about the sequence of a genome, the DNA molecule must be unzipped to form ssDNA, which possess different properties than dsDNA. Importantly, the persistent length of ssDNA is ~2 nm [107] which is roughly 25 times less than that of dsDNA. This is potentially troublesome, as herniation or hooking would be

able to occur in much more compact gels, which could lead to nanopore clogging, similar to the case of the agarose-interfaced nanopore with large DNA fragments. Furthermore, the R_g of the ssDNA would necessitate that the gel contain smaller pores as well. These two hurdles will be difficult to overcome, however through the use of a very tight gel, perhaps a carefully tuned version of polyacrylamide, would reduce the risk of clogging. Additionally, in the event of clogging, a computer program which monitors the current levels and reverses the voltage if an event is deemed to have taken too long could help free a trapped molecule, or even allow for multiple reads of the same section of DNA, lending itself to greater accuracy.

3.3 Final Thoughts

The use of a gel to slow down DNA passage in solid-state nanopores is a simple yet effective way to obtain a great amount of data for each passing molecule, without sacrificing the signal-to-noise ratio, or the capture rate. While the field moves towards making nanopores more clinically relevant, the issue of molecular translocation speed needs to be addressed. The method of using a *trans* side gel is not without its faults, such as adding complexity to the nanopore design, but it is a step in the right direction. Importantly, I was able to reduce the translocation speed of individual DNA molecules, both for long and short DNA fragments. With the further exploration and experimentation with various gel pore sizes, it is possible that we could help render the nanopore an asset for clinical applications.

References

[1] Allen, J. P., *The Art of Medicine in Ancient Egypt*, New York, **2005**.

[2] Clancy, S., *Nat. Educ.* **2008**, *1*, 102.

[3] Kranenburg, O., *Biochim. Biophys. Acta* **2005**, *1756*, 81.

[4] Hayden, E., *Nat. Publ. Gr.* **2014**.

[5] Shendure, J., Ji, H., *Nat. Biotechnol.* **2008**, *26*, 1135.

[6] Talaga, D. S., Li, J., *J. Am. Chem. Soc.* **2009**, 9287.

[7] Illumina, *System Specification Sheet: Sequencing - HiSeq X ™ Ten*, **2014**.

[8] Wanunu, M., *Phys. Life Rev.* **2012**, *9*, 125.

[9] Kulis, M., Esteller, M., *Adv. Genet.* **2010**, *70*, 27.

[10] Shim, J., Humphreys, G. I., Venkatesan, B. M., Munz, J. M., Zou, X., Sathe, C., Schulten, K., Kosari, F., Nardulli, A. M., Vasmatzis, G., Bashir, R., *Sci. Rep.* **2013**, *3*, 1389.

[11] Hayden, E., *Nat. Publ. Gr.* **2014**.

[12] Kowalczyk, S. W., Grosberg, A. Y., Rabin, Y., Dekker, C., *Nanotechnology* **2011**, *22*, 315101.

[13] Carlsen, A. T., Zahid, O. K., Ruzicka, J., Taylor, E. W., Hall, A. R., *ACS Nano* **2014**, *8*, 4754.

[14] Smeets, R. M. M., Keyser, U. F., Krapf, D., Wu, M.-Y., Dekker, N. H., Dekker, C., *Nano Lett.* **2006**, *6*, 89.

[15] Wanunu, M., *Phys. Life Rev.* **2013**, *9*, 125.

[16] Kwok, H., Briggs, K., Tabard-Cossa, V., *PLoS One* **2014**, *9*, e92880.

[17] B.H., *Pers. Commun. with Wanunu Gr.* **2015**.

[18] J.L., *Pers. Commun. with Wanunu Gr.* **2015**.

[19] S.C., *Pers. Commun. with Wanunu Gr.* **2015**.

[20] Beamish, E., Kwok, H., Tabard-Cossa, V., Godin, M., *Nanotechnology* **2012**, *23*, 405301.

[21] Branton, D., Deamer, D. W., Marziali, A., Bayley, H., Benner, S. A., Butler, T., Di Ventra, M., Garaj, S., Hibbs, A., Huang, X., Jovanovich, S. B., Krstic, P. S., Lindsay, S., Ling, X. S., Mastrangelo, C. H.,

Meller, A., Oliver, J. S., Pershin, Y. V, Ramsey, J. M., Riehn, R., Soni, G. V, Tabard-Cossa, V., Wanunu, M., Wiggin, M., Schloss, J. A., *Nat. Biotechnol.* **2008**, *26*, 1146.

[22] Deamer, D. W., Branton, D., *Acc. Chem. Res.* **2002**, *35*, 817.

[23] Grosberg, A. Y., Rabin, Y., *J. Chem. Phys.* **2010**, *133*, DOI 10.1063/1.3495481.

[24] Zwolak, M., Di Ventra, M., *Rev. Mod. Phys.* **2008**, *80*, 141.

[25] Deamer, D., *Annu. Rev. Biophys.* **2010**, *39*, 79.

[26] Lu, B., Albertorio, F., Hoogerheide, D. P., Golovchenko, J. a, *Biophys. J.* **2011**, *101*, 70.

[27] Balan, A., Machielse, B., Niedzwiecki, D., Lin, J., Ong, P., Engelke, R., Shepard, K. L., Drndic, M., **2014**.

[28] Waduge, P., Bilgin, I., Larkin, J., Henley, R. Y., Goodfellow, K., Graham, A. C., Bell, D. C., Vamivakas, N., Kar, S., Wanunu, M., **2015**, 7352.

[29] Meller, A., Nivon, L., Brandin, E., Golovchenko, J., Branton, D., *Proc. Natl. Acad. Sci. U. S. A.* **2000**, *97*, 1079.

[30] Fologea, D., Uplinger, J., Thomas, B., Mcnabb, D. S., Li, J., *Nano Lett.* **2005**, *5*, 1734.

[31] Kawano, R., Schibel, A. E. P., Cauley, C., White, H. S., *Langmuir* **2009**, *25*, 1233.

[32] Luan, B., Wang, D., Zhou, R., Harrer, S., Peng, H., Stolovitzky, G., *Nanotechnology* **2012**, *23*, 455102.

[33] Fologea, D., Uplinger, J., Thomas, B., McNabb, D. S., Li, J., *Nano Lett.* **2005**, *5*, 1734.

[34] Kowalczyk, S. W., Wells, D. B., Aksimentiev, A., Dekker, C., *Nano Lett.* **2012**, *12*, 1038.

[35] Hatlo, M. M., Panja, D., van Roij, R., *Phys. Rev. Lett.* **2011**, *107*, 068101.

[36] Wanunu, M., Morrison, W., Rabin, Y., Grosberg, A. Y., Meller, A., *Nat. Nanotechnol.* **2010**, *5*, 160.

[37] Zhang, H., Zhao, Q., Tang, Z., Liu, S., Li, Q., Fan, Z., Yang, F., You, L., Li, X., Zhang, J., Yu, D., *Small* **2013**, *9*, 4112.

[38] Lu, B., Hoogerheide, D. P., Zhao, Q., Zhang, H., Tang, Z., Yu, D., Golovchenko, J., *Nano Lett.* **2013**, *13*, 3048.

[39] Mitchell, N., Howorka, S., *Angew. Chem. Int. Ed. Engl.* **2008**, *120*, 5647.

[40] Cherf, G. M., Lieberman, K. R., Rashid, H., Lam, C. E., Karplus, K., Akeson, M., *Nat. Biotechnol.* **2012**, *30*, 344.

[41] Lieberman, K. R., Cherf, G. M., Doody, M. J., Olasagasti, F., Kolodji, Y., Akeson, M., *J. Am. Chem. Soc.* **2010**, *132*, 17961.

[42] Chu, J., González-López, M., Cockroft, S. L., Amorin, M., Ghadiri, M. R., *Angew. Chem. Int. Ed. Engl.* **2010**, *49*, 10106.

[43] Cockroft, S. L., Chu, J., Amorin, M., Ghadiri, M. R., *J. Am. Chem. Soc.* **2008**, *130*, 818.

[44] Hornblower, B., Coombs, A., Whitaker, R. D., Kolomeisky, A., Picone, S. J., Meller, A., Akeson, M., *Nat. Methods* **2007**, *4*, 315.

[45] Derrington, I. M., Butler, T. Z., Collins, M. D., Manrao, E., Pavlenok, M., Niederweis, M., Gundlach, J. H., *Proc. Natl. Acad. Sci. U. S. A.* **2010**, *107*, 16060.

[46] Manrao, E. A., Derrington, I. M., Laszlo, A. H., Langford, K. W., Hopper, M. K., Gillgren, N., Pavlenok, M., Niederweis, M., Gundlach, J. H., *Nat. Biotechnol.* **2012**, *30*, 349.

[47] Mathé, J., Visram, H., Viasnoff, V., Rabin, Y., Meller, A., *Biophys. J.* **2004**, *87*, 3205.

[48] Dudko, O. K., Mathé, J., Szabo, A., Meller, A., Hummer, G., *Biophys. J.* **2007**, *92*, 4188.

[49] Vercoutere, W., Winters-Hilt, S., Olsen, H., Deamer, D., Haussler, D., Akeson, M., *Nat. Biotechnol.* **2001**, *19*, 248.

[50] Olasagasti, F., Lieberman, K. R., Benner, S., Cherf, G. M., Dahl, J. M., Deamer, D. W., Akeson, M., *Nat. Nanotechnol.* **2010**, *5*, 798.

[51] Wiggin, M., Tropini, C., Tabard-Cossa, V., Jetha, N. N., Marziali, A., *Biophys. J.* **2008**, *95*, 5317.

[52] Jetha, N. N., Feehan, C., Wiggin, M., Tabard-Cossa, V., Marziali, A., *Biophys. J.* **2011**, *100*, 2974.

[53] Nakane, J., Wiggin, M., Marziali, A., *Biophys. J.* **2004**, *87*, 615.

[54] Van den Hout, M., Vilfan, I. D., Hage, S., Dekker, N. H., *Nano Lett.* **2010**, *10*, 701.

[55] Keyser, U. F., Koeleman, B. N., van Dorp, S., Krapf, D., Smeets, R. M. M., Lemay, S. G., Dekker, N. H., Dekker, C., *Nat. Phys.* **2006**, *2*, 473.

[56] Peng, H., Ling, X. S., *Nanotechnology* **2009**, *20*, 185101.

[57] Hyun, C., Kaur, H., Rollings, R., Xiao, M., Li, J., *ACS Nano* **2013**, *7*, 5892.

[58] Wanunu, M., Sutin, J., McNally, B., Chow, A., Meller, A., *Biophys. J.* **2008**, *95*, 4716.

[59] Kurz, V., Nelson, E. M., Shim, J., Timp, G., *ACS Nano* **2013**, *7*, 4057.

[60] Briggs, K., Kwok, H., Tabard-Cossa, V., *Small* **2014**, *10*, 2077.

[61] Di Fiori, N., Squires, A., Bar, D., Gilboa, T., Moustakas, T. D., Meller, A., *Nat. Nanotechnol.* **2013**, *8*, 946.

[62] Krishnakumar, P., Gyarfas, B., Song, W., Sen, S., Zhang, P., Krstić, P., Lindsay, S., *ACS Nano* **2013**, *7*, 10319.

[63] Yusko, E. C., Johnson, J. M., Majd, S., Prangkio, P., Rollings, R. C., Li, J., Yang, J., Mayer, M., *Nat. Nanotechnol.* **2011**, *6*, 253.

[64] Anderson, B. N., Muthukumar, M., Meller, A., *ACS Nano* **2013**, *7*, 1408.

[65] He, Y., Tsutsui, M., Scheicher, R. H., Bai, F., Taniguchi, M., Kawai, T., *ACS Nano* **2013**, *7*, 538.

[66] Belkin, M., Maffeo, C., Wells, D. B., Aksimentiev, A., *ACS Nano* **2013**, *7*, 6816.

[67] Luan, B., Peng, H., Polonsky, S., Rossnagel, S., Stolovitzky, G., Martyna, G., *Phys. Rev. Lett.* **2010**, *104*, 238103.

[68] Polonsky, S., Rossnagel, S., Stolovitzky, G., *Appl. Phys. Lett.* **2007**, *91*, 153103.

[69] Ai, Y., Liu, J., Zhang, B., Qian, S., *Anal. Chem.* **2010**, *82*, 8217.

[70] Paik, K., Liu, Y., Tabard-cossa, V., Waugh, M. J., Huber, D. E., Provine, J., Howe, R. T., Dutton, R. W., Davis, R. W., *ACS Nano* **2012**, *6*, 6767.

[71] Liu, Y., Huber, D. E., Tabard-Cossa, V., Dutton, R. W., *Appl. Phys. Lett.* **2010**, *97*, 143109.

[72] He, Y., Tsutsui, M., Fan, C., Taniguchi, M., Kawai, T., *ACS Nano* **2011**, *5*, 5509.

[73] Yen, P., Wang, C., Hwang, G.-J., Chou, Y. C., *Rev. Sci. Instrum.* **2012**, *83*, 034301.

[74] Tsutsui, M., He, Y., Furuhashi, M., Rahong, S., Taniguchi, M., Kawai, T., *Sci. Rep.* **2012**, *2*, 394.

[75] Tsutsui, M., Rahong, S., Iizumi, Y., Okazaki, T., Taniguchi, M., Kawai, T., *Sci. Rep.* **2011**, *1*, 46.

[76] Squires, A. H., Hersey, J. S., Grinstaff, M. W., Meller, A., *J. Am. Chem. Soc.* **2013**, *135*, 16304.

[77] Manning, G. S., *J. Chem. Phys.* **1969**, *51*, 3249.

[78] Ghosal, S., *Phys. Rev. Lett.* **2007**, *98*, 1.

[79] Grønbech-Jensen, N., Mashl, R., Bruinsma, R., Gelbart, W., *Phys. Rev. Lett.* **1997**, *78*, 2477.

[80] Barz, D. P. J., Ehrhard, P., *Lab Chip* **2005**, *5*, 949.

[81] Tabard-cossa, V., Wiggin, M., Trivedi, D., Jetha, N. N., Dwyer, J. R., Marziali, A., **2009**, *3*, 3009.

[82] Lang, D., Bujard, H., Wolff, B., Russell, D., *J. Mol. Biol.* **1967**, *23*, 163.

[83] Viovy, J., *Rev. Mod. Phys.* **2000**, *72*, 813.

[84] Chanda, M., *Introduction to Polymer Science and Chemistry: A Problem-Solving Approach*, CRC Press, **2013**.

[85] Tree, D. R., Muralidhar, A., Doyle, P. S., Dorfman, K. D., *Macromolecules* **2013**, *46*, 8369.

[86] Landers, J. P., *Capillary and Microchip Electrophoresis and Associated Microtechniques*, CRC Press, **2007**.

[87] Stellwagen, N. C., *Electrophoresis* **2009**, *30*, S188.

[88] Griess, G. a, Moreno, E. T., Easom, R. a, Serwer, P., *Biopolymers* **1989**, *28*, 1475.

[89] Pernodet, N., Tinland, B., Sadron, I. C., Pasteur, C. L., *Electrophoresis* **1997**, 55.

[90] Hayashi, A., Kinoshita, K., Kuwano, M., *Polym. J.* **1977**, *9*, 219.

[91] Tobita, H., Hamielec, a. E., *Polymer (Guildf).* **1990**, *31*, 1546.

[92] Ando, G., Hyun, C., Li, J., Mitsui, T., *ACS Nano* **2012**, *6*, 10090.

[93] Venkatesan, B. M., Bashir, R., *Nat. Nanotechnol.* **2011**, *6*, 615.

[94] Zhang, X., Wang, Y., Fricke, B. L., Gu, L., *ACS Nano* **2014**, *8*, 3444.

[95] Singer, A., Rapireddy, S., Ly, D. H., Meller, A., *Nano Lett.* **2012**, *12*, 1722.

[96] Kang, X., Cheley, S., Rice-Ficht, A. C., Bayley, H., *J. Am. Chem. Soc.* **2007**, *129*, 4701.

[97] Briggs, K., Charon, M., Kwok, H., Le, T., Chahal, S., Bustamante, J., Waugh, M., Tabard-Cossa, V., *Nanotechnology* **2015**, *26*, 084004.

[98] Holmes, D. L., Stellwagen, N. C., *Electrophoresis* **1990**, *11*, 5.

[99] Maaloum, M., Pernodet, N., Tinland, B., *Electrophoresis* **1998**, *19*, 1606.

[100] Fatin-Rouge, N., Milon, A., Buffle, J., Goulet, R. R., Tessier, A., *J. Phys. Chem. B* **2003**, *107*, 12126.

[101] Piculell, L., Nilsson, S., *J. Phys. Chem.* **1989**, *93*, 5602.

[102] Wanunu, M., Sutin, J., Meller, A., *Nano Lett.* **2009**, *9*, 3498.

[103] Starchev, K., Sturm, J., Weill, G., Brogren, C.-H., *J. Phys. Chem. B* **1997**, *101*, 5659.

[104] Fatin-Rouge, N., Starchev, K., Buffle, J., *Biophys. J.* **2004**, *86*, 2710.

[105] Saxton, M. J., *Biophys. J.* **1994**, *66*, 394.

[106] Plesa, C., van Loo, N., Ketterer, P., Dietz, H., Dekker, C., *Nano Lett.* **2015**, *15*, 732.

[107] Chi, Q., Wang, G., Jiang, J., *Phys. A Stat. Mech. its Appl.* **2013**, *392*, 1072.

[108] Tabard-Cossa, V., Trivedi, D., Wiggin, M., Jetha, N. N., Marziali, A., *Nanotechnology* **2007**, *18*, 305505.

[109] Tabard-Cossa, V., *Engineered Nanopores for Bioanalytical Applications*, Elsevier, **2013**.

[110] Skinner, G. M., van den Hout, M., Broekmans, O., Dekker, C., Dekker, N. H., *Nano Lett.* **2009**, *9*, 2953.